

NAVAL POSTGRADUATE SCHOOL
Monterey, California



THESIS

**MULTI-LEVEL TECHNIQUE FOR STIFFNESS AND
STRENGTH CALCULATIONS OF WOVEN FABRIC
COMPOSITE PLATE AND SHELL STRUCTURES**

by

Ahmet Altekin

June 2001

Thesis Advisor:

Young W. Kwon

Approved for public release; distribution is unlimited

20011108 165

| | | | | |
|--|---|--|---|--|
| REPORT DOCUMENTATION PAGE | | | <i>Form Approved OMB No. 0704-0188</i> | |
| Public reporting burden for this collection of information is estimated to average 1 hour per response, including the time for reviewing instruction, searching existing data sources, gathering and maintaining the data needed, and completing and reviewing the collection of information. Send comments regarding this burden estimate or any other aspect of this collection of information, including suggestions for reducing this burden, to Washington headquarters Services, Directorate for Information Operations and Reports, 1215 Jefferson Davis Highway, Suite 1204, Arlington, VA 22202-4302, and to the Office of Management and Budget, Paperwork Reduction Project (0704-0188) Washington DC 20503. | | | | |
| 1. AGENCY USE ONLY (Leave blank) | 2. REPORT DATE JUNE 2001 | 3. REPORT TYPE AND DATES COVERED Master's Thesis | | |
| 4. TITLE AND SUBTITLE: Multi-level Technique For Stiffness And Strength Calculations Of Woven Fabric Composite Plate And Shell Structures | | | 5. FUNDING NUMBERS | |
| 6. AUTHOR (S) Altekin,Ahmet | | | | |
| 7. PERFORMING ORGANIZATION NAME(S) AND ADDRESS(ES) Naval Postgraduate School Monterey, CA 93943-5000 | | | 8. PERFORMING ORGANIZATION REPORT NUMBER | |
| 9. SPONSORING / MONITORING AGENCY NAME (S) AND ADDRESS (ES) N/A | | | 10. SPONSORING / MONITORING AGENCY REPORT NUMBER | |
| 11. SUPPLEMENTARY NOTES The views expressed in this thesis are those of the author and do not reflect the official policy or position of the Department of Defense or the U.S. Government. | | | | |
| 12a. DISTRIBUTION / AVAILABILITY STATEMENT Approved for public release; distribution is unlimited | | | 12b. DISTRIBUTION CODE | |
| 13. ABSTRACT The stiffness and strength behavior of the woven fabric composite materials mainly depend on the properties of the fiber and matrix materials. A technique was developed to design and analyze woven fabric composites based on the micro-level properties of the fiber and matrix materials. The technique is based on the bilateral relationships among the fiber/matrix materials, the unidirectional composite (strand), the woven fabric layer and the laminated composite structure as in the given order. Simplified and efficient analytical models were developed for the relationship between any subsequent levels of woven fabric composite materials. The technique is used to predict the structural level stiffness and strength in terms of material and the geometric configuration of the woven fabric and lamination. Progressive damage or failure can also be simulated at the fiber and matrix level by using this technique. | | | | |
| 14. SUBJECT TERMS Multilevel Technique, Woven Fabric Composite, Fiber, Matrix, Strand, Volume Fraction, Damage Size, Undulation Angle, Failure Criteria | | | 15. NUMBER OF PAGES 78 | |
| | | | 16. PRICE CODE | |
| 17. SECURITY CLASSIFICATION OF REPORT Unclassified | 18. SECURITY CLASSIFICATION OF THIS PAGE Unclassified | 19. SECURITY CLASSIFICATION OF ABSTRACT Unclassified | 20. LIMITATION OF ABSTRACT UL | |

THIS PAGE INTENTIONALLY LEFT BLANK

Approved for public release; distribution is unlimited

**MULTI-LEVEL TECHNIQUE FOR STIFFNESS AND STRENGTH
CALCULATIONS OF WOVEN FABRIC COMPOSITE PLATE AND SHELL
STRUCTURES**

Ahmet Altekin
Lieutenant Junior Grade, Turkish Navy
B.S. Mechanical Engineering, Turkish Naval Academy, 1994

Submitted in partial fulfillment of the
requirements for the degree of

MASTER OF SCIENCE IN MECHANICAL ENGINEERING

from the

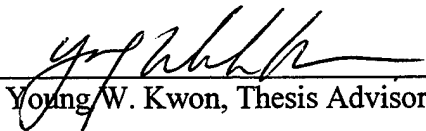
**NAVAL POSTGRADUATE SCHOOL
June 2001**

Author:

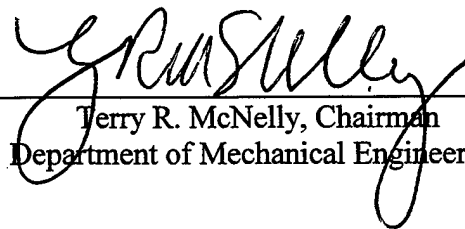


Ahmet Altekin

Approved by:



Young W. Kwon, Thesis Advisor



Terry R. McNelly, Chairman
Department of Mechanical Engineering

THIS PAGE INTENTIONALLY LEFT BLANK

ABSTRACT

The stiffness and strength behavior of the woven fabric composite materials mainly depend on the properties of the fiber and matrix materials. A technique was developed to design and analyze woven fabric composites based on the micro-level properties of the fiber and matrix materials. The technique is based on the bilateral relationships among the fiber/matrix materials, the unidirectional composite (strand), the woven fabric layer and the laminated composite structure as in the given order. Simplified and efficient analytical models were developed for the relationship between any subsequent levels of woven fabric composite materials. The technique is used to predict the structural level stiffness and strength in terms of material and the geometric configuration of the woven fabric and lamination. Progressive damage or failure can also be simulated at the fiber and matrix level by using this technique.

THIS PAGE INTENTIONALLY LEFT BLANK

TABLE OF CONTENTS

| | | |
|-------------|---|-----------|
| I. | INTRODUCTION..... | 1 |
| II. | BACKGROUND | 5 |
| A. | LITERATURE SURVEY..... | 5 |
| III. | MULTILEVEL TECHNIQUE..... | 9 |
| A. | MODELLING AND FORMULATION..... | 9 |
| 1. | Fiber-Strand Module..... | 12 |
| 2. | Strand-Fabric Module..... | 16 |
| 3. | Lamination Module | 21 |
| B. | FAILURE CRITERIA AT THE CONSTITUENT LEVEL..... | 21 |
| VI. | NUMERICAL SOLUTION VERIFICATION | 23 |
| V. | RESULTS AND DISCUSSION | 25 |
| A. | PLATE SUBJECTED TO IN -PLANE LOADING..... | 25 |
| 1. | Effect of Fiber Volume Fraction (V^f) on The Fiber Failure Stress | 26 |
| 2. | Effect of Damage Size on the Fiber Failure Stress..... | 26 |
| B. | PLATES SUBJECTED TO BENDING LOADS | 29 |
| 1. | Clamped Plates..... | 29 |
| 2. | Simply Supported Plates | 37 |
| C. | EFFECTS OF E_F, V^F_S AND θ_U ON THE MAXIMUM FIBER STRESS..... | 42 |
| D. | FAILURE PROGRESS..... | 46 |
| E. | SHELL STRUCTURES SUBJECTED TO BENDING LOADS | 48 |
| VI. | CONCLUSION AND RECOMMENDATIONS..... | 55 |
| | LIST OF REFERENCES..... | 57 |
| | INITIAL DISTRIBUTION LIST..... | 59 |

THIS PAGE INTENTIONALLY LEFT BLANK

LIST OF FIGURES

| | |
|---|----|
| Figure 1. Examples of Woven Fabrics: a) plain weave ($n_g=2$), b) twill weave ($n_g=3$), c) four harness satin ($n_g=4$)..... | 3 |
| Figure 2. Multi-level Approach to Woven-Fabric Composite Structures..... | 11 |
| Figure 3. Fiber-Strand Unit Cell Model..... | 15 |
| Figure 4. Strand-Fabric Unit-Cell Model for a Plain Weave Composite | 20 |
| Figure 5. Mesh Generation with 100 Linear Triangular Elements | 25 |
| Figure 6. Volume Fraction vs. Normalized Failure Stress..... | 27 |
| Figure 7. Normalized Damaged Element Size vs. Normalized Failure Stress | 28 |
| Figure 8. Mesh Generation with (5x5) Four Nodded Quadrilateral Elements | 32 |
| Figure 9. Square Plate, Clamped Edges, Concentrated Load at The Center, | 33 |
| Fiber Stress Plot..... | 33 |
| Figure 10. Square Plate, Clamped Edges, Concentrated Load at The Center, | 33 |
| Fiber Stress Contour Plot..... | 33 |
| Figure 11. Square Plate, Clamped Edges, Uniformly Distributed Load,..... | 34 |
| Fiber Stress Plot..... | 34 |
| Figure 12. Square Plate, Clamped Edges, Uniformly Distributed Load,..... | 34 |
| Fiber Stress Contour Plot..... | 34 |
| Figure 13. Rectangular Plate, Clamped Edges, Concentrated Load at The Center, Fiber Stress Plot..... | 35 |
| Figure 14. Rectangular Plate, Clamped Edges, Concentrated Load at The Center, Fiber Stress Contour Plot | 35 |
| Figure 15. Rectangular Plate, Clamped Edges, Uniformly Distributed Load, Fiber Stress Plot..... | 36 |
| Figure 16. Rectangular, Clamped Edges, Uniformly Distributed Load, Fiber Stress Contour Plot..... | 36 |
| Figure 17. Square Plate, Simply Supported Edges, Concentrated Load at The Center, Fiber Stress Plot..... | 38 |
| Figure 18. Square Plate, Simply Supported Edges, Concentrated Load at The Center, Fiber Stress Contour Plot..... | 38 |
| Figure 19. Square Plate, Simply Supported Edges, Uniformly Distributed Load, Fiber Stress Plot..... | 39 |
| Figure 20. Square Plate, Simply Supported Edges, Uniformly Distributed Load, Fiber Stress Contour Plot | 39 |
| Figure 21. Rectangular Plate, Simply Supported Edges, Concentrated Load at The Center, Fiber Stress Plot..... | 40 |
| Figure 22. Rectangular Plate, Simply Supported Edges, Concentrated Load at The Center, Fiber Stress Contour Plot..... | 40 |
| Figure 23. Rectangular Plate, Simply Supported Edges, Uniformly Distributed Load, Fiber Stress Plot..... | 41 |
| Figure 24. Rectangular Plate, Simply Supported Edges, Uniformly Distributed Load, Fiber Stress Contour Plot..... | 41 |

| | |
|--|----|
| Figure 25. Elastic Modulus vs. Maximum Fiber Stress..... | 43 |
| Figure 26. Fiber Volume Fraction vs. Maximum Fiber Stress | 44 |
| Figure 27. Undulation Angle vs. Maximum Fiber Stress | 45 |
| Figure 28. Maximum Fiber Stress Occurs at the Center and Failure Initiates at That Point... | 47 |
| Figure 29. Failure at The Center Gets Bigger Catastrophically and The Whole Structure Fails..... | 47 |
| Figure 30. Cylinder Shaped Shell Structure Meshed with 400(20x20) Equilateral Elements..... | 49 |
| Figure 31. Fiber Stress Distribution Along The Cylinder-Shaped Structure, Bending Load at Point P1 | 50 |
| Figure 32. Fiber Stress Distribution Along The Cylinder-Shaped Structure, Bending Load at Point P2..... | 52 |
| Figure 33. Fiber Stress Distribution Along The Cylinder Shaped Structure, Bending Load at Point P3..... | 53 |

LIST OF TABLES

| | |
|--|----|
| Table 1: Properties of Fiber and Matrix Materials..... | 23 |
| Table 2: Properties of Strand Material..... | 24 |
| Table 3: Material Properties of Strands and Resin | 24 |
| Table 4: Comparison of Plain Weave Composite Made of Carbon/Epoxy | 24 |
| Table 5: Comparison of Plain Weave Composite Made of E-Glass/Vinylester..... | 24 |
| Table 6: Plain Weave, Woven Fabric Composite..... | 24 |

THIS PAGE INTENTIONALLY LEFT BLANK

ACKNOWLEDGEMENTS

I would like to express my gratitude to Professor Young W. Kwon for his guidance and assistance in the completion of this research, and for making my time at The Naval Postgraduate School enjoyable, challenging but most of all rewarding.

Sincere appreciation is due my loving wife Atike, whose love, devotion and support is never ending and is the foundation of my success in life and in my career.

THIS PAGE INTENTIONALLY LEFT BLANK

I. INTRODUCTION

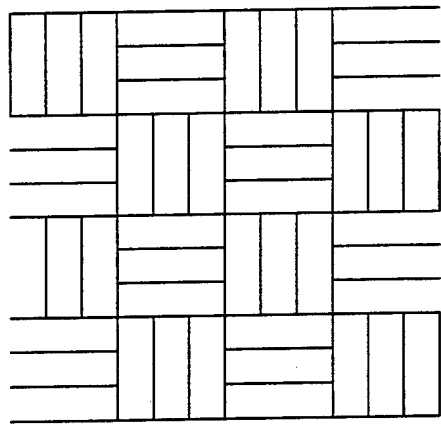
The interest in composite materials has been growing steadily in recent years. The use of composite materials in the fields of aeronautics and naval construction for the fabrication of high mechanical performance structures is increasing day by day. One of the most commonly used composites is woven fabric composite, in which strands are formed by many different ways of weaving, resulting in different stiffness and strength. The ease of handling and low fabrication cost have made woven fabric composite materials attractive. However, the geometry of this composite class is complex, and the choice of architectures, constituents and models is unlimited.

Most woven composites are made of two sets of interlaced threads, known as the warp (vertical) and fill (horizontal) threads. The term interlaced is used to indicate where the fill and warp threads cross over each other. The warp and fill threads and interlaced region for a woven composite are shown in Figure 1.

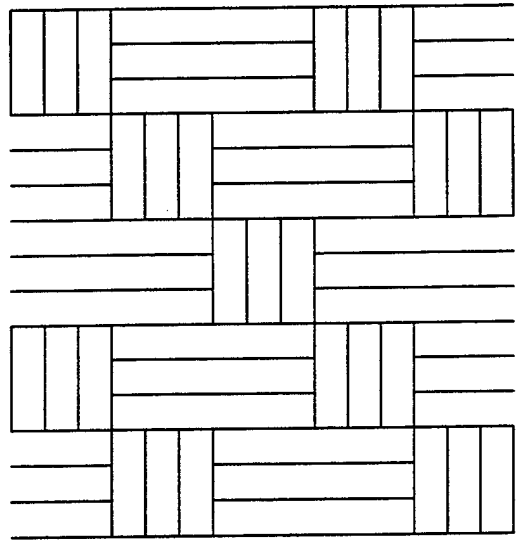
The numerous types of weaves can be defined by the repeating patterns in both warp and fill directions, defined by the n_g^F and n_g^W . The number of n_g^F indicates that a warp thread is interlaced with every n_g^F -th fill thread and n_g^W means that a fill thread is interlaced with every n_g^W -th warp thread. For most of the woven composites $n_g^F = n_g^W = n_g$. Because in most of the woven fabrics, only one type of fiber material is used, material parameters like thread width ratio and relative fiber volume fraction are not used. Woven fabrics with $n_g \geq 4$ and with interlaced regions that are not connected are known as satin weaves. As defined by their n_g values, the fabrics in Figure 1 are known as *plain weave* ($n_g=2$), *twill weave* ($n_g=3$), *four harness satin* ($n_g=4$).

Much research has been done on plain weave composites particularly on the effective stiffness of such composites. There is a growing need to develop techniques for the analysis of woven fabric composite structures from the known mechanical properties of constituent phases. In order to predict the effective material properties of woven composites, plate lamination theories have been used using orthotropic yarn materials that were made of unidirectional fibers and matrix. [Ref.1-Ref.8]. Less attention has been given to the strength prediction of woven composites.

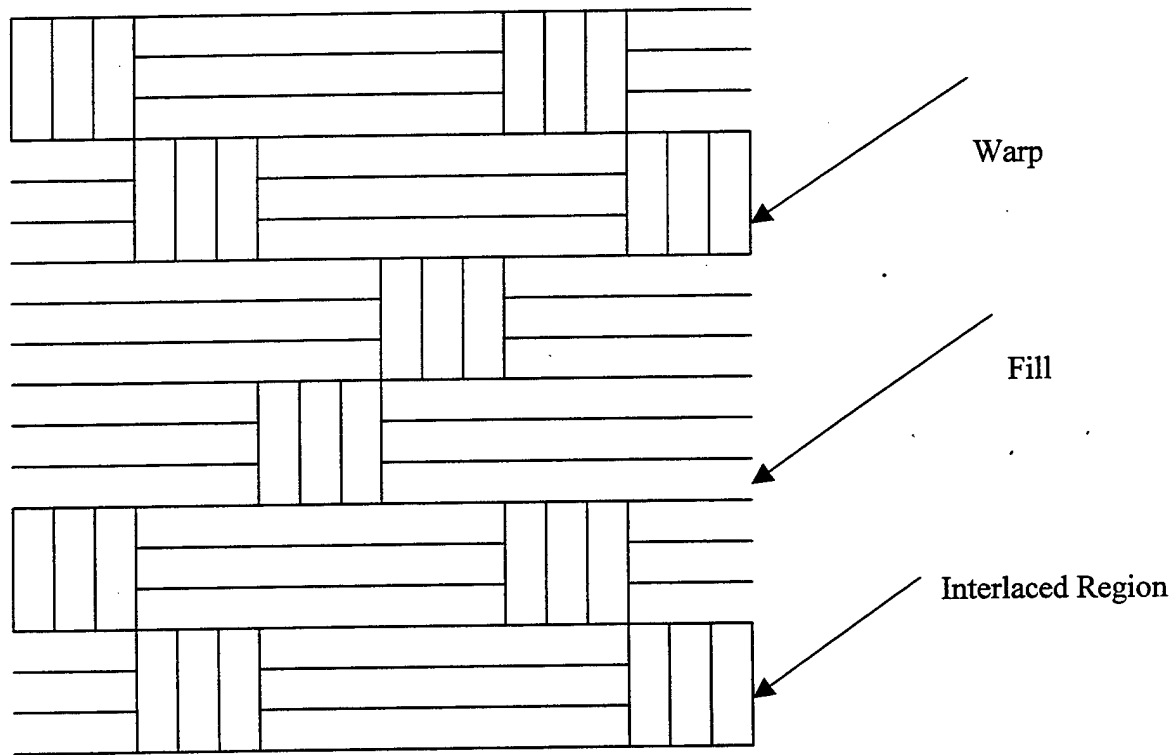
In this study, a new multi-level, micro/macro modeling for a woven fabric composite is presented. The technique can be used to predict the maximum stress under a certain load conditions and to simulate progressive damage of a woven fabric composite by using finite element formulation. This technique has a similar structure to the one described in [Ref. 9]. However, the present modeling approach is much simpler and computationally more efficient.



(a)



(b)



(c)

Figure 1. Examples of Woven Fabrics: a) plain weave ($n_g=2$), b) twill weave ($n_g=3$), c) four harness satin ($n_g=4$)

THIS PAGE INTENTIONALLY LEFT BLANK

II. BACKGROUND

A. LITERATURE SURVEY

An extensive amount of research has been conducted to gain better understanding of woven composite materials. This is important because the improvement of woven fabric composite material properties depends on understanding and characterization of the basic reinforcing micro-mechanisms, interaction effects between the various constituents and the role of fiber distribution for failure progress.

Ishikawa and Chou [Ref. 1] developed the mosaic model that was based on the assumptions of constant stress and constant strain. They also conducted an approximate analysis by taking into account the fiber undulation and continuity. Two dimensional finite element analyses support their mosaic and undulation theory.

Zhang and Harding [Ref. 6] tried to solve the problem of the micro-mechanics analysis of the elastic constants of a one-ply plain weave composite using the strain energy equivalency principle with the aid of the finite element method.

Large number of studies was conducted to determine the effective material properties from the constituent materials and their geometry. As a result of these studies many different models have been developed. Most of these studies like Mosaic Model of Ishikawa and Chou [Ref. 2] and MESOTEX of Scida, D., Aboura, Z., Benzeggagh, M.M., and Boscherens, E [Ref. 3] focus on the one-way passage from the constituent material level to the unidirectional fiber composite. However, the other passage to decompose strains and stress into the fiber and matrix level is important if failure or damage criteria are to be applied at the constituent material level. Thus, some of previous works developed the bi-passage models.[Ref. 12-Ref. 18]. Aboudi [Ref. 12] and Kwon and his

co-workers [Ref. 13-Ref. 15] used the unit cell model for the analytical bi-directional module. Aboudi's model was mathematically elegant and Kwon's model had a compact expression for computational efficiency. Pechold and Rahman [Ref. 16] used the strength of material approach with equivalent springs. Their model was very simple but neglected the interaction of Poisson's effects of the fibers and the matrix. Hansen and his co-workers [Ref. 17-Ref. 18] used another approach for the bi-directional model. However their model can not compute the effective composite material properties from constituent data directly. As a result, they used an independent finite element analysis at the micro level to determine effective composite properties.

Many researchers have also studied the relations between orthotropic properties of the unidirectional fiber-matrix composite and the effective material properties of the woven fabric composite. In order to predict the effective material properties of woven fabric composite, four fundamental homogenization methods have been used in the past: strain energy balance, plate approximation, direct method with area averaging and asymptotic expansion homogenization.

Strain energy balance methods exert a uniform average strain while complementary energy methods apply a uniform average stress. The asymptotic expansion homogenization approach explicitly employs periodic boundary conditions to simulate the condition of global periodicity of the microstructure. Vandeurzen, Ivens and Verpoest [Ref. 9] proposed a Combi Cell Method (CCM) for a general weave geometry which is capable of predicting 3D stress state at constituent level which does not invoke isostrain or isostress condition throughout the unit cell. Garnich and Hansen [Ref. 17]

suggested Multi-Continuum Theory (MCT). This bridged the structural analysis to micro-mechanics.

THIS PAGE INTENTIONALLY LEFT BLANK

III. MULTILEVEL TECHNIQUE

A. MODELLING AND FORMULATION

The proposed multi-level continuum analysis for laminated, woven-fabric composite structures is sketched in Figure 2. The analysis consists of three modules. The purpose of the first module (called *Fiber-Strand* in Figure 2) is to relate the constituent materials (i.e. the fiber and the matrix materials) to the smeared unidirectional composite (strand) material. The purpose of the second module (called *Strand-Fabric*) is to connect the unidirectional composite (strand) material to the woven fabric material. The third module (called *Lamination*) is designed to bridge between the woven fabric material and the laminated composite structure for which the finite element analysis is performed.

Each module has bi-directional passage from one side to the other. In other words, each module computes effective material properties from the lower level material properties, and decomposes the upper level strains into the lower level strains. Ultimately, the multi-level analysis determines the stresses and strains at the fiber and matrix level so that failure or damage criteria can be applied to the constituent materials.

The overall procedure of the multi-level continuum analysis is explained below for analyses of laminated woven fabric composite structures.

1. Compute the effective material properties for the finite element structural analysis using the three modules described above, starting from the fiber and matrix properties.
2. For a load increment, compute the response of the structure such as deformation and strains from the finite element analysis.

3. Apply the three modules from top to bottom to compute stresses and strains at the fiber and matrix level.
4. Apply failure or damage criteria to check potential failure or damage at the constituent material level such as fiber breakage, matrix cracking, and interface failure.
5. Once there is failure or damage, degrade the material properties of the failed or damaged location and compute the effective composite properties using the three modules for the next step of finite element structural analysis. If there is no failure, the effective properties calculated in #1 can be used for the next finite element analysis.
6. The computation continues iteratively until the composite structure fails or the designated final load is reached.

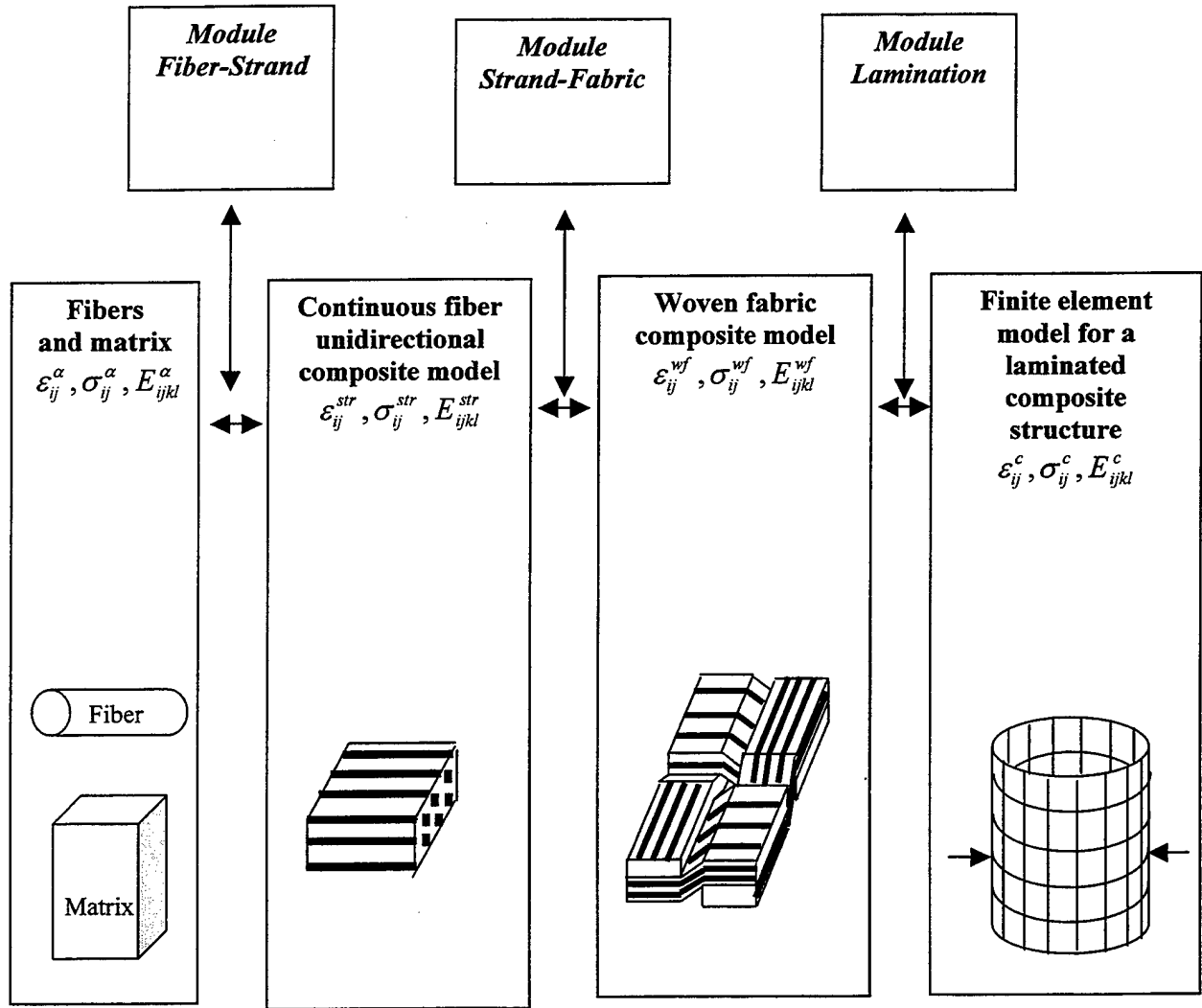


Figure 2. Multi-level Approach to Woven-Fabric Composite Structures

1. Fiber-Strand Module

The fiber-strand module relates the constituent materials, e.g. the fiber and matrix, to the smeared unidirectional composite (strand). Because the fiber and the matrix are the base units for composite structures, this module is at the lowest level in the analysis. The fiber-strand module has two functions; the first function is to compute the effective material properties of the unidirectional composite (strand) using the fiber and matrix properties. The second function is to decompose the strains and stresses at the strand level to those at the fiber and matrix level so that progressive damage or failure can be evaluated at the fiber and matrix level. Thus, the Module *Fiber-Strand* establishes the bi-directional relationship between the constituent materials and the unidirectional composite (strand).

A unit cell is made of a fiber and surrounding matrix material. The fiber represents the average behavior of many fibers in the area under consideration, and is assumed to have a square shape of cross-section. Because of symmetry, a quarter of the unit cell is considered as shown in Figure 3. In the figure, axis 1 is the fiber direction, and axes 2 and 3 are normal to the fiber direction. The quarter unit cell has four sub-cells and the size of the sub-cell depends on the fiber volume fraction.

The following derivation is for the normal components of stresses and strains. Stress equilibrium at the sub-cell interfaces is expressed in terms of average values for each sub-cell as below:

$$\sigma_{22}^a = \sigma_{22}^b, \quad \sigma_{22}^c = \sigma_{22}^d, \quad \sigma_{33}^a = \sigma_{33}^c, \quad \sigma_{33}^b = \sigma_{33}^d \quad (1)$$

$$\sigma_{12}^a = \sigma_{12}^b, \quad \sigma_{12}^c = \sigma_{12}^d, \quad \sigma_{13}^a = \sigma_{13}^c, \quad \sigma_{13}^b = \sigma_{13}^d \quad (2)$$

$$\sigma_{23}^a = \sigma_{23}^b, \sigma_{23}^b = \sigma_{23}^c, \sigma_{23}^c = \sigma_{23}^d, \quad (3)$$

where subscripts denote stress components and the superscript indicates sub-cells, as shown in Figure 3.

Compatibility of deformation is assumed for strain components as is given below:

$$\varepsilon_{11}^a = \varepsilon_{11}^b, \varepsilon_{11}^b = \varepsilon_{11}^c, \varepsilon_{11}^c = \varepsilon_{11}^d \quad (4)$$

$$\sqrt{v^f} \varepsilon_{22}^a + (1 - \sqrt{v^f}) \varepsilon_{22}^b = \sqrt{v^f} \varepsilon_{22}^c + (1 - \sqrt{v^f}) \varepsilon_{22}^d \quad (5)$$

$$\sqrt{v^f} \varepsilon_{33}^a + (1 - \sqrt{v^f}) \varepsilon_{33}^c = \sqrt{v^f} \varepsilon_{33}^b + (1 - \sqrt{v^f}) \varepsilon_{33}^d \quad (6)$$

$$\varepsilon_{12}^a + \varepsilon_{12}^b = \varepsilon_{12}^c + \varepsilon_{12}^d \quad (7)$$

$$\varepsilon_{13}^a + \varepsilon_{13}^c = \varepsilon_{13}^b + \varepsilon_{13}^d \quad (8)$$

in which v^f is the fiber volume fraction.

The unit cell (i.e. strand) stresses and strains are related to the sub-cell (i.e. fiber and matrix) stresses and strains as below:

$$\sigma_{ij}^{str} = v^f \sigma_{ij}^a + \sqrt{v^f} (1 - \sqrt{v^f}) \sigma_{ij}^b + \sqrt{v^f} (1 - \sqrt{v^f}) \sigma_{ij}^c + (1 - \sqrt{v^f})^2 \sigma_{ij}^d \quad (9)$$

$$\varepsilon_{ij}^{str} = v^f \varepsilon_{ij}^a + \sqrt{v^f} (1 - \sqrt{v^f}) \varepsilon_{ij}^b + \sqrt{v^f} (1 - \sqrt{v^f}) \varepsilon_{ij}^c + (1 - \sqrt{v^f})^2 \varepsilon_{ij}^d \quad (10)$$

These equations state that the strand stresses and strains are volumetric averages of sub-cell stresses and strains, respectively.

The constitutive equation for each sub-cell can be expressed as:

$$\sigma_{ij}^\alpha = E_{ijkl}^\alpha \varepsilon_{kl}^\alpha \quad (i, j, k, l = 1, 2, 3 \text{ and } \alpha = a, b, c, d) \quad (11)$$

where superscript α denotes the respective sub-cell of fiber or matrix, and E_{ijkl}^{α} is the material property tensor. The hygro-thermal effects are not included in Eq. (11), but they can be easily implemented in the equation as shown in [Ref. 13].

Proper algebraic manipulations of the previous equations finally result in:

$$[E^{str}] = [V][E][R_2] \quad (12)$$

$$\{\varepsilon^{\alpha}\} = [R_2]\{\varepsilon^{str}\} \quad (13)$$

Where $[V]$ is the matrix containing volume fractions of each sub-cell, $[E]$ is the matrix consisting of material properties of the fiber and matrix, and $[R_2]$ is the matrix to decompose the strand strains $\{\varepsilon^{str}\}$ into the fiber and matrix strains $\{\varepsilon^{\alpha}\}$. Equation (12) computes the effective material property matrix $[E^{str}]$ for the strand and it is the path from the constituent level to the strand level.

Conversely, Eq. (13) is the path from the strand level to the constituent material level. Therefore, these two equations establish the bi-directional relationship in the fiber-strand module and the fiber and matrix stresses are computed from Eqs. (11) and (13).

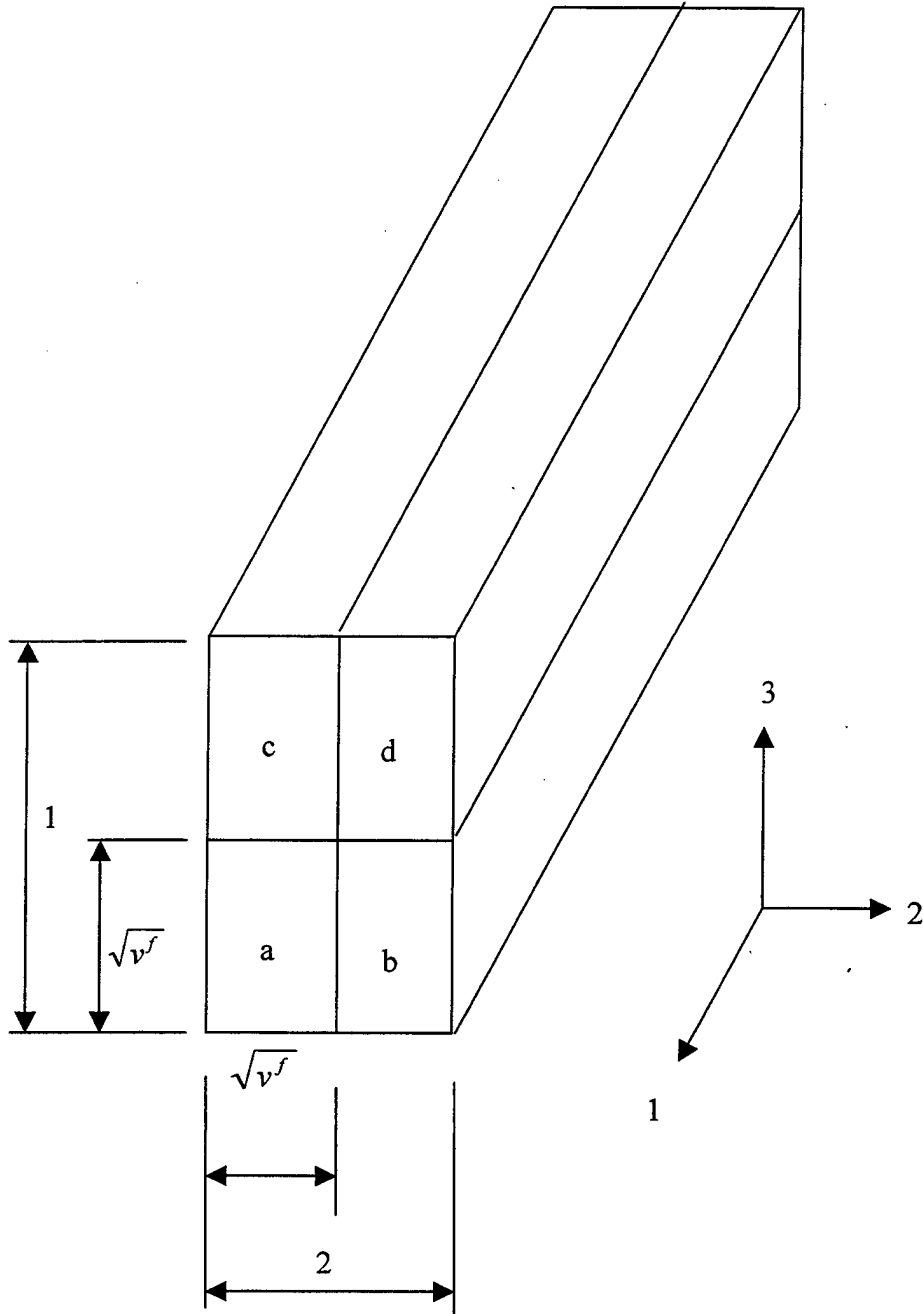


Figure 3. Fiber-Strand Unit Cell Model

2. Strand-Fabric Module

The strand-fabric module relates material properties of a unidirectional strand to the effective material properties of the woven fabric composite. Like the previous module, this module has two functions: computation of the effective properties of the woven fabric using the strand materials and their weaving information, and decomposition of the woven strains and stresses into the strand strains and stresses.

Here, the strand-fabric module is developed for a plain weave composite. The plain weave composite model is presented in Figure 4. The model has 13 sub-cells, and most of those sub-cells have fibers along the axis-1 or 2 direction. On the other hand, four sub-cells (#2, 4, 6, and 8 in Figure 4) have fibers in inclined orientations, and sub-cell #5 is filled with the matrix material.

First of all, the normal stress/strain components are discussed below. There are three normal strains for each sub-cell with the total of 39 strains ($(\varepsilon_{kl}^{str})^n$, $n=1, 2, \dots, 13$). There are three normal strains at the unit-cell level (ε_{kl}^{wf}). Those strains represent the average values of each sub-cell or the unit-cell, respectively. In order to relate them, equilibrium and compatibility conditions are applied. At respective interfaces between any two neighboring sub-cells, the normal stresses on the interface plane should be in equilibrium.

$$(\sigma_{11}^{str})^1 = (\sigma_{11}^{str})^2, (\sigma_{11}^{str})^2 = (\sigma_{11}^{str})^{11}, (\sigma_{11}^{str})^3 = (\sigma_{11}^{str})^{10}, (\sigma_{11}^{str})^4 = (\sigma_{11}^{str})^5, \quad (14)$$

$$(\sigma_{11}^{str})^5 = (\sigma_{11}^{str})^6, (\sigma_{11}^{str})^7 = (\sigma_{11}^{str})^{13}, (\sigma_{11}^{str})^8 = (\sigma_{11}^{str})^9, (\sigma_{11}^{str})^9 = (\sigma_{11}^{str})^{12}, \quad (15)$$

$$(\sigma_{22}^{str})^1 = (\sigma_{22}^{str})^{12}, (\sigma_{22}^{str})^4 = (\sigma_{22}^{str})^{10}, (\sigma_{22}^{str})^4 = (\sigma_{22}^{str})^7, (\sigma_{22}^{str})^2 = (\sigma_{22}^{str})^5, \quad (16)$$

$$(\sigma_{22}^{str})^5 = (\sigma_{22}^{str})^8, (\sigma_{22}^{str})^3 = (\sigma_{22}^{str})^6, (\sigma_{22}^{str})^6 = (\sigma_{22}^{str})^{13}, (\sigma_{22}^{str})^9 = (\sigma_{22}^{str})^{11}, \quad (17)$$

$$(\sigma_{33}^{str})^1 = (\sigma_{33}^{str})^{10}, (\sigma_{33}^{str})^3 = (\sigma_{33}^{str})^{11}, (\sigma_{33}^{str})^7 = (\sigma_{33}^{str})^{12}, (\sigma_{33}^{str})^9 = (\sigma_{33}^{str})^{13} \quad (18)$$

where the superscript denotes the sub-cell numbers in Figure 4 and the subscript indicates the stress components. In addition, some strain compatibility conditions are assumed for a uniform deformation.

$$(\varepsilon_{11}^{str})^1 + (\varepsilon_{11}^{str})^{11} = (\varepsilon_{11}^{str})^3 + (\varepsilon_{11}^{str})^{10}, \quad (19)$$

$$a_1(\varepsilon_{11}^{str})^{10} + b_1(\varepsilon_{11}^{str})^2 + a_1(\varepsilon_{11}^{str})^3 = a_1(\varepsilon_{11}^{str})^4 + b_1(\varepsilon_{11}^{str})^5 + a_1(\varepsilon_{11}^{str})^6, \quad (20)$$

$$a_1(\varepsilon_{11}^{str})^4 + b_1(\varepsilon_{11}^{str})^5 + a_1(\varepsilon_{11}^{str})^6 = a_1(\varepsilon_{11}^{str})^7 + b_1(\varepsilon_{11}^{str})^8 + a_1(\varepsilon_{11}^{str})^{13}, \quad (21)$$

$$(\varepsilon_{11}^{str})^7 + (\varepsilon_{11}^{str})^{13} = (\varepsilon_{11}^{str})^9 + (\varepsilon_{11}^{str})^{12}, \quad (22)$$

$$(\varepsilon_{22}^{str})^1 + (\varepsilon_{22}^{str})^{12} = (\varepsilon_{22}^{str})^7 + (\varepsilon_{22}^{str})^{10}, \quad (23)$$

$$a_2(\varepsilon_{22}^{str})^{10} + b_2(\varepsilon_{22}^{str})^4 + a_2(\varepsilon_{22}^{str})^7 = a_2(\varepsilon_{22}^{str})^2 + b_2(\varepsilon_{22}^{str})^5 + a_2(\varepsilon_{22}^{str})^8, \quad (24)$$

$$a_2(\varepsilon_{22}^{str})^2 + b_2(\varepsilon_{22}^{str})^5 + a_2(\varepsilon_{22}^{str})^8 = a_2(\varepsilon_{22}^{str})^3 + b_2(\varepsilon_{22}^{str})^6 + a_2(\varepsilon_{22}^{str})^{13} \quad (25)$$

$$(\varepsilon_{22}^{str})^3 + (\varepsilon_{22}^{str})^{13} = (\varepsilon_{22}^{str})^9 + (\varepsilon_{22}^{str})^{11}, \quad (26)$$

$$t_1(\varepsilon_{33}^{str})^1 + t_2(\varepsilon_{33}^{str})^{10} = (t_1 + t_2)(\varepsilon_{33}^{str})^2, \quad (27)$$

$$t_1(\varepsilon_{33}^{str})^3 + t_2(\varepsilon_{33}^{str})^{11} = (t_1 + t_2)(\varepsilon_{33}^{str})^2, \quad (28)$$

$$t_1(\varepsilon_{33}^{str})^3 + t_2(\varepsilon_{33}^{str})^{11} = (t_1 + t_2)(\varepsilon_{33}^{str})^4, \quad (29)$$

$$(\varepsilon_{33}^{str})^4 = (\varepsilon_{33}^{str})^5, \quad (30)$$

$$(\varepsilon_{33}^{str})^5 = (\varepsilon_{33}^{str})^6, \quad (31)$$

$$t_1(\varepsilon_{33}^{str})^7 + t_2(\varepsilon_{33}^{str})^{12} = (t_1 + t_2)(\varepsilon_{33}^{str})^6, \quad (32)$$

$$t_1(\varepsilon_{33}^{str})^7 + t_2(\varepsilon_{33}^{str})^{12} = (t_1 + t_2)(\varepsilon_{33}^{str})^8, \quad (33)$$

$$t_1(\varepsilon_{33}^{str})^9 + t_2(\varepsilon_{33}^{str})^{13} = (t_1 + t_2)(\varepsilon_{33}^{str})^8, \quad (34)$$

Here, a_i , b_i , and t_i are the dimensions of the plain weave construction as shown in Figure 4. Finally, the unit-cell strain and stress are assumed to be the volume average of the sub-cell strains and stresses, respectively. That is,

$$\varepsilon_{ij}^{wf} = \sum_{n=1}^{13} V^n (\varepsilon_{ij}^{str})^n \quad (35)$$

$$\sigma_{ij}^{wf} = \sum_{n=1}^{13} V^n (\sigma_{ij}^{str})^n \quad (36)$$

Here, V^n is the volume fraction of the n^{th} sub-cell. The constitutive equation for each sub-cell is expressed as:

$$(\sigma_{ij}^{str})^n = (E_{ijkl}^{str})^n (\varepsilon_{kl}^{str})^n \quad (i, j, k, l = 1, 2, 3) \quad (37)$$

Where the summation sign convention is applied only to the subscripts, k and l . For each sub-cell, $(E_{ijkl}^{str})^n$ should be determined based on the orientation of the strand inside the sub-cell. Algebraic manipulation of the previous equations, (i.e, Eqs. (14) through (37)) yields the following relationship:

$$E_{ijkl}^{wf} = f\left((E_{ijkl}^{str})^n, a_i, b_i, t_i\right) \quad (38)$$

$$(\varepsilon_{ij}^{str})^n = g\left(\varepsilon_{ij}^{wf}, a_i, b_i, t_i\right) \quad (39)$$

Equations (38) and (39) are equivalent to Eqs. (12) and (13) for the fiber-strand module, respectively. Equation (38) computes the effective material properties of the woven fabric composite based on the material and geometric properties of the strands while. Eq. (39) calculates the strains at the strand level from the woven fabric strains. Once the strand strains are computed, strand stresses can be computed from the constituent equations.

A similar derivation can be made for shear components. For example, the shear component parallel to 1-2 plane can be derived as shown below. The shear stress equilibrium at the sub-cell interfaces is written as

$$t_1(\sigma_{12}^{str})^1 + t_2(\sigma_{12}^{str})^{10} = (t_1 + t_2)(\sigma_{12}^{str})^2, \quad (40)$$

$$t_1(\sigma_{12}^{str})^3 + t_2(\sigma_{12}^{str})^{11} = (t_1 + t_2)(\sigma_{12}^{str})^2, \quad (41)$$

$$t_1(\sigma_{12}^{str})^1 + t_2(\sigma_{12}^{str})^{10} = (t_1 + t_2)(\sigma_{12}^{str})^4, \quad (42)$$

$$t_1(\sigma_{12}^{str})^7 + t_2(\sigma_{12}^{str})^{13} = (t_1 + t_2)(\sigma_{12}^{str})^4, \quad (43)$$

$$t_1(\sigma_{12}^{str})^7 + t_2(\sigma_{12}^{str})^{12} = (t_1 + t_2)(\sigma_{12}^{str})^7, \quad (44)$$

$$t_1(\sigma_{12}^{str})^9 + t_2(\sigma_{12}^{str})^{13} = (t_1 + t_2)(\sigma_{12}^{str})^8, \quad (45)$$

$$t_1(\sigma_{12}^{str})^9 + t_2(\sigma_{12}^{str})^{13} = (t_1 + t_2)(\sigma_{12}^{str})^6, \quad (46)$$

$$(\sigma_{12}^{str})^2 = (\sigma_{12}^{str})^5, \quad (47)$$

Assumed strain compatibility expressions are:

$$(\varepsilon_{12}^{str})^1 = (\varepsilon_{12}^{str})^{10}, \quad (48)$$

$$(\varepsilon_{12}^{str})^3 = (\varepsilon_{12}^{str})^{11}, \quad (49)$$

$$(\varepsilon_{12}^{str})^7 = (\varepsilon_{12}^{str})^{12}, \quad (50)$$

$$(\varepsilon_{12}^{str})^3 = (\varepsilon_{12}^{str})^9. \quad (51)$$

Use of Eqs. (40) through (51) along with Eqs. (35) through (37) for the shear component yields the shear component part of Eqs. (38) and (39).

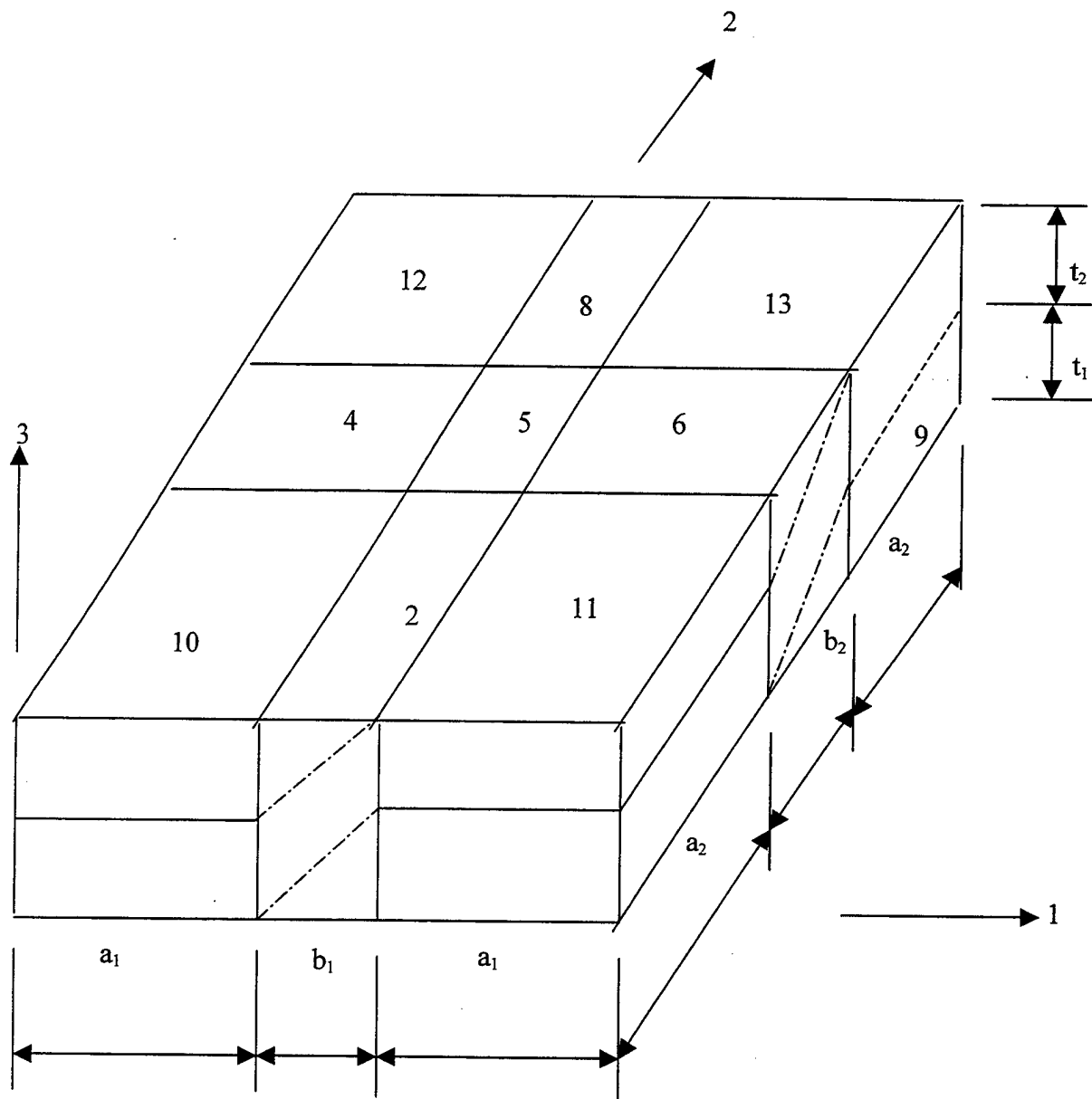


Figure 4. Strand-Fabric Unit-Cell Model for a Plain Weave Composite

3. Lamination Module

The lamination module eventually bridges the effective material properties of a woven fabric lamina and the finite element analysis of the composite structure. Depending on the types of finite elements used, the connection would be different. For laminated composite structures, the woven lamina properties may be applied to the finite element analysis program, or smeared properties of several laminates may be pre-calculated for the finite element program using a lamination theory. In this study, the shear deformable Mindlin-Reissner plate bending theory is used. The theory includes transverse shear deformation and calculates the smeared material properties of a laminate.

B. FAILURE CRITERIA AT THE CONSTITUENT LEVEL

Failure in a composite structure is described in terms of base materials, the fiber, matrix and interface. Thus, failure can be classified as fiber failure, matrix failure and interface failure at the constituent material level. Since fibers are long and slender, compressive failure of the fibers is quite different from tensile failure. Thus, four failure are considered: fiber failure in tension, fiber failure in compression, matrix failure, and interface failure.

These failure modes at the fiber and matrix level can represent various modes at the structural level such as delamination, fiber splitting, and matrix cracking. Once there is a failure, the corresponding material properties are degraded accordingly. Depending on the material behavior of each constituent and their interface, proper failure criteria need to be selected. For example, an isotropic failure criterion is chosen for an isotropic matrix material.

THIS PAGE INTENYIONALLY LEFT BLANK

VI. NUMERICAL SOLUTION VERIFICATION

First of all, the fiber-strand module and the strand-fabric module were tested independently. The fiber-strand module was validated extensively in previous works [Ref.13-15] and it was tested again for a carbon/epoxy strand. The fiber and matrix materials are shown in Table 1. The effective stiffness and strength properties of the strand made of the fiber and matrix materials in Table 1 and with a fiber volume fraction of 0.7 are compared to the results in [Ref. 19] in Table 2.

Plain weave composites were studied using the strand-fabric module. (Material properties of the strands of the woven-fabric composites are tabulated in Table 3.) The calculated effective material properties are compared to other results in Tables 4 and 5 for the carbon/epoxy and e-glass/vinylester woven composites, respectively. The present results compared well to other experimental data or analytical results.

Another plain weave composite made of the strand in Table 2 was also studied for its tensile strength. The predicted strength using the fiber-strand and strand-fabric modules is compared to the test result in [Ref. 19]. As shown in Table 6, the predicted strength agrees well with the test result

Table 1: Properties of Fiber and Matrix Materials

| | E_1 (GPa) | E_2 (GPa) | G_{12} (GPa) | G_{23} (GPa) | γ_{12} | γ_{23} | Tensile Strength (MPa) | Shear Strength (MPa) |
|--------|----------------|----------------|-------------------|-------------------|---------------|---------------|------------------------------|----------------------------|
| Fiber | 221.0 | 3.8 | 13.8 | 5.5 | 20 | 25 | 3585 | |
| Matrix | 4.4 | 4.4 | 1.6 | 1.6 | 0.34 | 0.34 | 159 | 100 |

Table 2: Properties of Strand Material

| | E_1 (GPa) | E_2 (GPa) | γ_{12} | γ_{23} | Longitudinal Strength (MPa) | Transverse Strength (MPa) |
|-----------|----------------|----------------|---------------|---------------|-----------------------------------|---------------------------------|
| Ref. [19] | 151.0 | 10.1 | 0.24 | 0.50 | 2550 | 152 |
| Present | 156.0 | 10.2 | 0.24 | 0.54 | 2543 | 148 |

Table 3: Material Properties of Strands and Resin

| | E_1 (GPa) | E_2 (GPa) | G_{12} (GPa) | G_{23} (GPa) | γ_{12} | γ_{23} |
|--------------------|-------------|-------------|----------------|----------------|---------------|---------------|
| E-Glass/Vinylester | 57.5 | 18.8 | 7.44 | 7.26 | 0.25 | 0.29 |
| Carbon/Epoxy | 134 | 10.2 | 5.52 | 3.43 | 0.30 | 0.49 |
| Epoxy | 3.45 | 3.45 | 1.28 | 1.28 | 0.35 | 0.35 |

Table 4: Comparison of Plain Weave Composite Made of Carbon/Epoxy

| | E_1 (GPa) | E_2 (GPa) | G_{12} (GPa) | G_{23} (GPa) | γ_{12} | γ_{23} |
|-----------------|-------------|-------------|----------------|----------------|---------------|---------------|
| Exp. [Ref. 20] | 55.5 | --- | 4.93 | --- | 0.0 | --- |
| Result [Ref. 5] | 56.1 | 10.4 | 5.08 | 3.71 | 0.03 | 0.59 |
| Present Result | 54.9 | 10.2 | 4.28 | 3.47 | 0.02 | 0.47 |

Table 5: Comparison of Plain Weave Composite Made of E-Glass/Vinylester

| | E_1 (GPa) | E_2 (GPa) | G_{12} (GPa) | G_{23} (GPa) | γ_{12} | γ_{23} |
|-----------------|----------------|---------------|----------------|----------------|----------------|-----------------|
| Exp. [Ref. 3] | 24.8 ± 1.1 | 8.5 ± 2.6 | 6.5 ± 0.8 | 4.2 ± 0.7 | 0.1 ± 0.01 | 0.28 ± 0.07 |
| Result [Ref. 3] | 25.3 | 13.4 | 5.19 | 5.24 | 0.12 | 0.29 |
| Present Result | 24.4 | 12.4 | 5.92 | 4.52 | 0.12 | 0.28 |

Table 6: Plain Weave, Woven Fabric Composite

| | Tensile Strength (MPa) |
|-----------|------------------------|
| Present | 753 |
| Ref. [19] | 750 |

V. RESULTS AND DISCUSSION

A. PLATE SUBJECTED TO IN-PLANE LOADING

In this section, square shaped woven fabric plates, subjected to uniaxial in-plane loading, are examined for fiber failure stress. Because of symmetry, one quarter of the plates was modeled. The plates are plain weave composites. The fiber and matrix materials are listed in Table 1. The square shaped plates are meshed with 100 linear triangular elements. The finite element mesh can be seen in Figure 5. The longitudinal fiber stresses are calculated at every element.

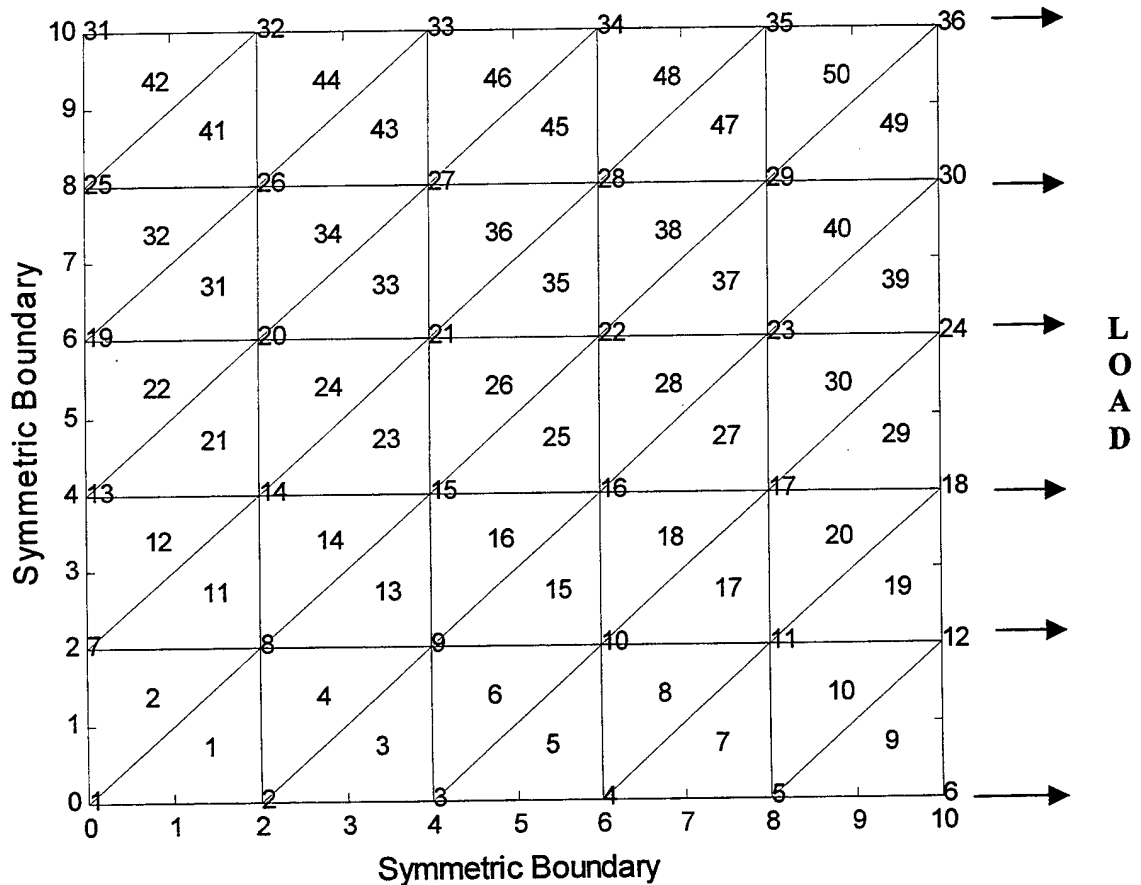


Figure 5. Mesh Generation with 100 Linear Triangular Elements

1. Effect of Fiber Volume Fraction (V^f) on The Fiber Failure Stress

Composite material properties depend upon the properties of fiber and matrix materials of which they are made. The fiber volume fraction is the percentage of the volume of composite material that is occupied by the fiber. Fibers are major load-carrying elements in a structure under load. As a result, in this set of studies the effect of fiber volume fraction on the fiber stress is examined for the in-plane loaded woven fabric composites.

Figure 6 shows the variation of the maximum fiber stress in a composite as a function of the fiber volume fraction. The maximum fiber stress is normalized with respect to the value when the fiber volume fraction is 0.7. Increasing the volume fraction up to $V^f=0.7$ increases the failure stresses linearly. After $V^f=0.7$ increasing V^f results in a nonlinear decrease in normalized failure stress.

2. Effect of Damage Size on the Fiber Failure Stress

For this set of studies the elements on one of the symmetric edges are assumed to be damaged, and the effect of damage size on the fiber stress is examined. The damaged elements have the reduction of material properties by a factor of 100. The maximum fiber stress of the woven composite with the volume fraction $V^f=0.7$, and no damage condition is selected for normalization of the computed fiber stresses. Figure 7 shows the fiber stress variation with along with the damage size which is normalized with respect to the whole length of the symmetric edge. The normalized fiber stress shows a non-linear decrease with increasing damaged size.

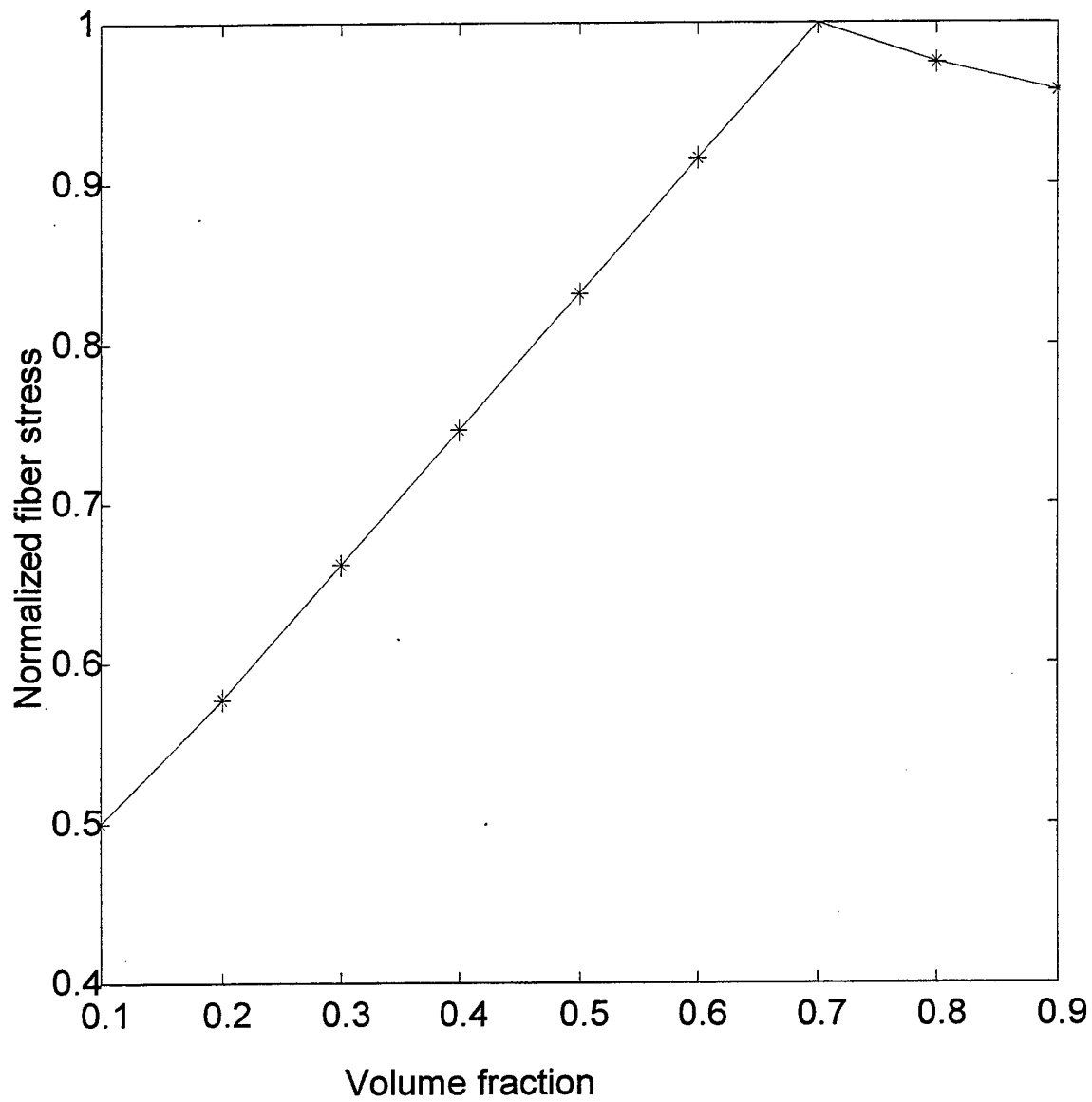


Figure 6. Volume Fraction vs. Normalized Failure Stress

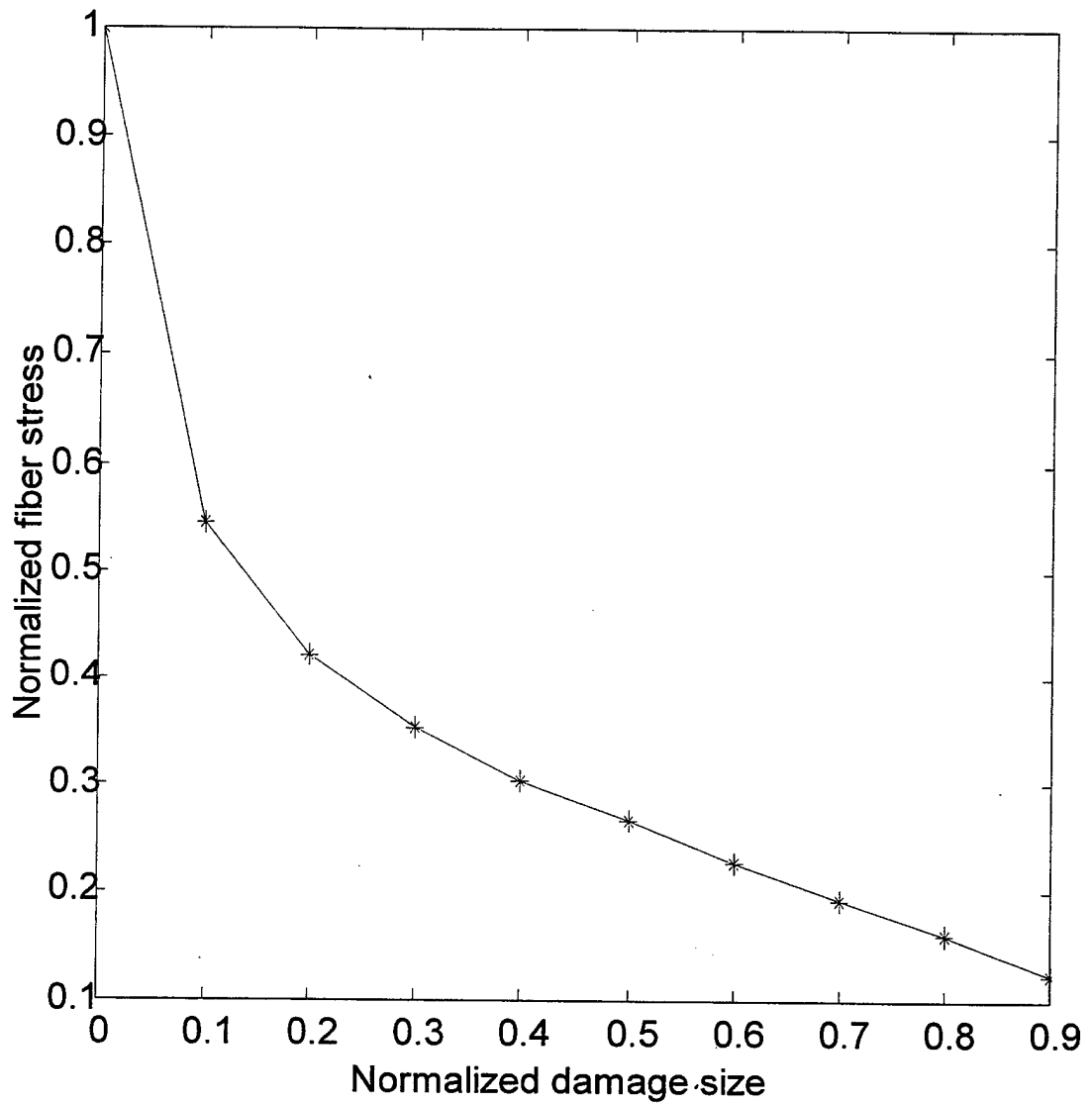


Figure 7. Normalized Damaged Element Size vs. Normalized Failure Stress

B. PLATES SUBJECTED TO BENDING LOADS

1. Clamped Plates

In this section of the study, woven fabric plates of two different geometries (square, rectangle) with the same surface areas, 20x20, 10x40, are examined for the condition of clamped edges, under bending loads. All composite plates are plain weave composites. The fiber and matrix materials are listed in Table 1 and the fiber volume fraction of the material is 0.5. Because of symmetry, quarters of the plates are modeled. The quarter plates are meshed with 25 (5x5) four-node quadrilateral elements. The mesh is shown in Figure 8. For the two different geometries, plates are subjected to concentrated transverse loads at the center and distributed pressure loads, respectively. The longitudinal fiber stresses are computed at the Gauss integration points of every element due to the fact that fibers are ultimate load carrying members. The distribution of fiber stress along the plates can be seen in Figures 9-26. The fiber stresses are normalized for the applied unit force.

Plots show that different geometries and load applications result in different fiber stress values and stress distributions. For the square plate subjected to a concentrated center load, the maximum fiber stress occurs at the center, and the minimum fiber stress occurs at the corners of the plate. The fiber stress decreases from the center toward the symmetric boundary until the $2/3$ distance between the center and edge. Then, the stress starts to increase toward the symmetry edge where the fiber stress is approximately $2/3$ of the maximum fiber stress at the center. Due to the symmetric boundary conditions and equal length of edges, the stress distribution is symmetric along the diagonal direction of

the plate. The stress distribution for the concentrated center load is shown in Figures 9-10.

Distributed load creates the maximum fiber stress at the center of the clamped boundaries. The fiber stress at the center is lower than the stress at the clamped edge but it is the location of next large fiber stress. The maximum stress caused by the concentrated load is approximately 5 times greater than the maximum stress created by the distributed load. The stress distribution for the distributed load can be seen in Figures 11-12.

For the rectangular plate subjected to a concentrated center load, the maximum fiber stress occurs at the center again while minimum stress occurs at the clamped edges farther away from the center. The fiber stress decreases from the center toward the clamped edges closer to the center until the midpoint between the edge and center, and then it increases up to a stress value at the edge, which is very close to maximum stress at the center. The fiber stress is negligible on about the half of the plate surface near the clamped boundaries farther away from the center. The stress distribution for the concentrated center load is shown in Figures 13-14.

For the distributed load, the maximum fiber stress does not occur at the center but it occurs at the middle of long clamped edges. The fiber stress remains almost constant along the long clamped edges until the half of the distance. Then, the stress decreases almost linearly along these long edges and it becomes zero at the corners. The maximum fiber stress under the uniform load is 8 times less than the maximum stress under the concentrated load. The stress distribution for the distributed load can be seen in Figures 15-16.

For both rectangular and square plates subjected to concentrated and distributed loads, respectively, with clamped edges, maximum fiber stress values are almost the same.

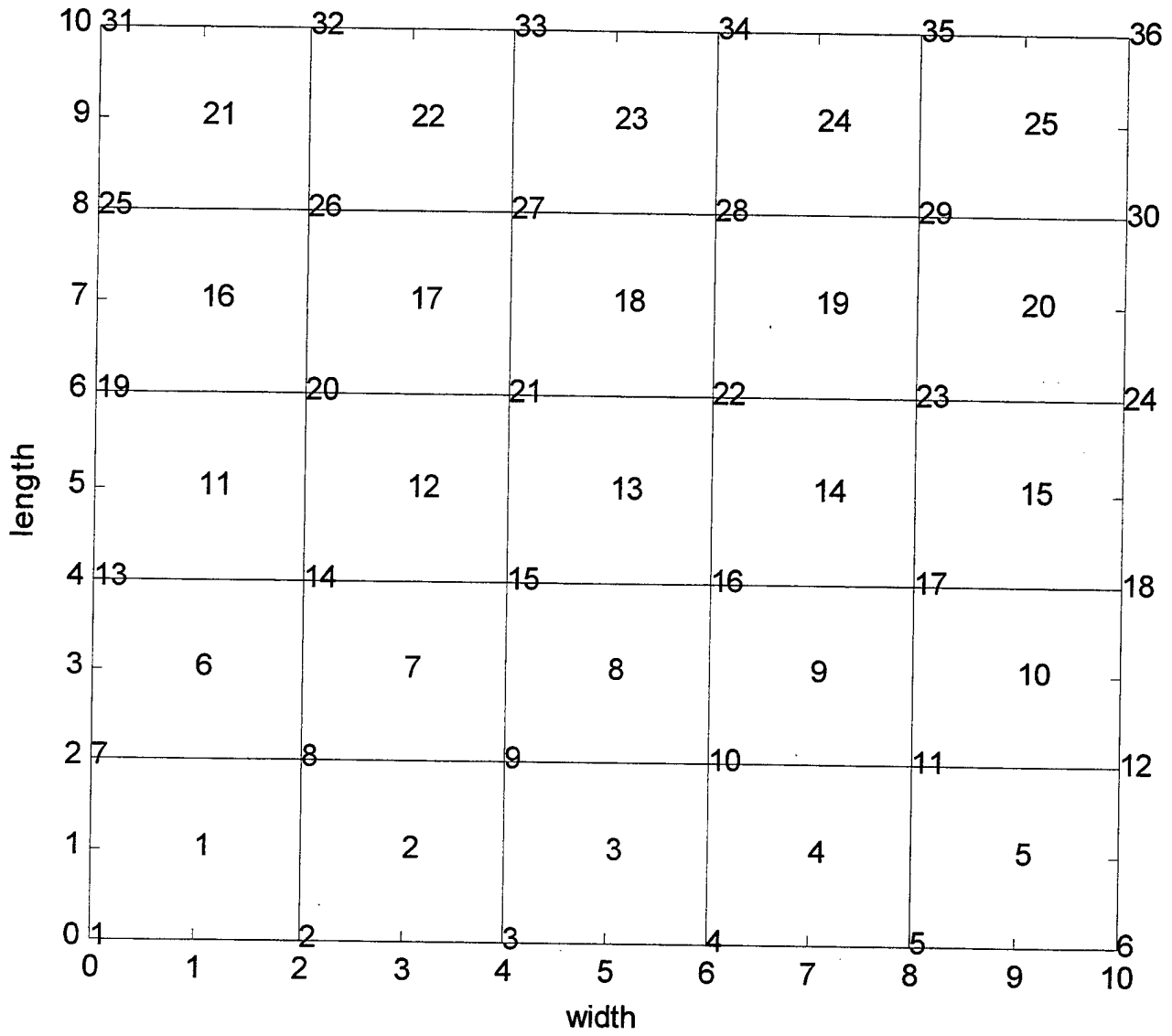


Figure 8. Mesh Generation with (5x5) Four Nodded Quadrilateral Elements

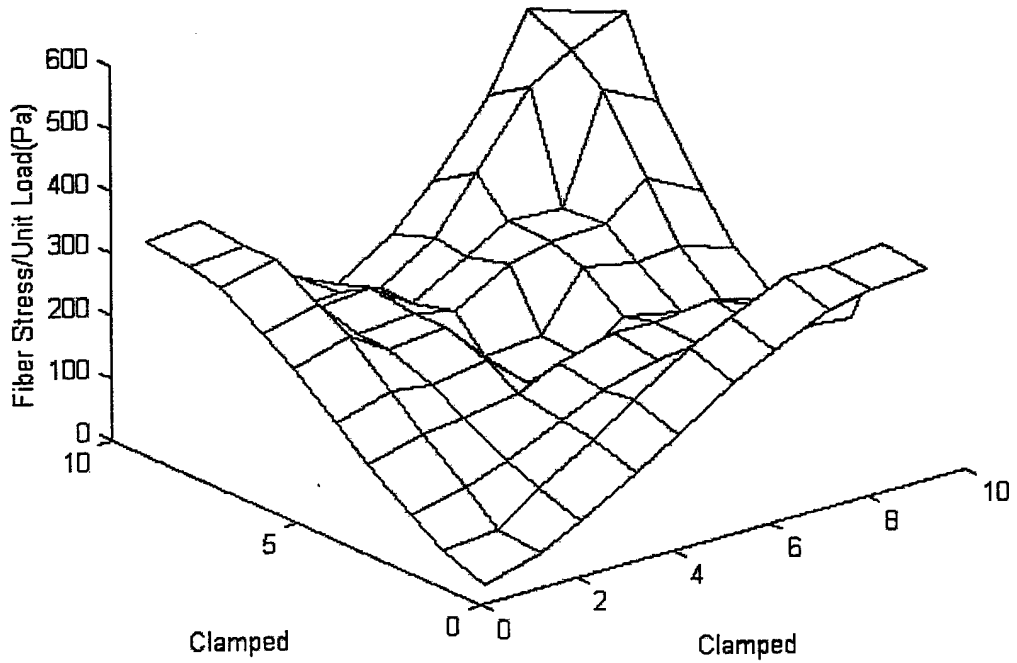


Figure 9. Square Plate, Clamped Edges, Concentrated Load at The Center, Fiber Stress Plot

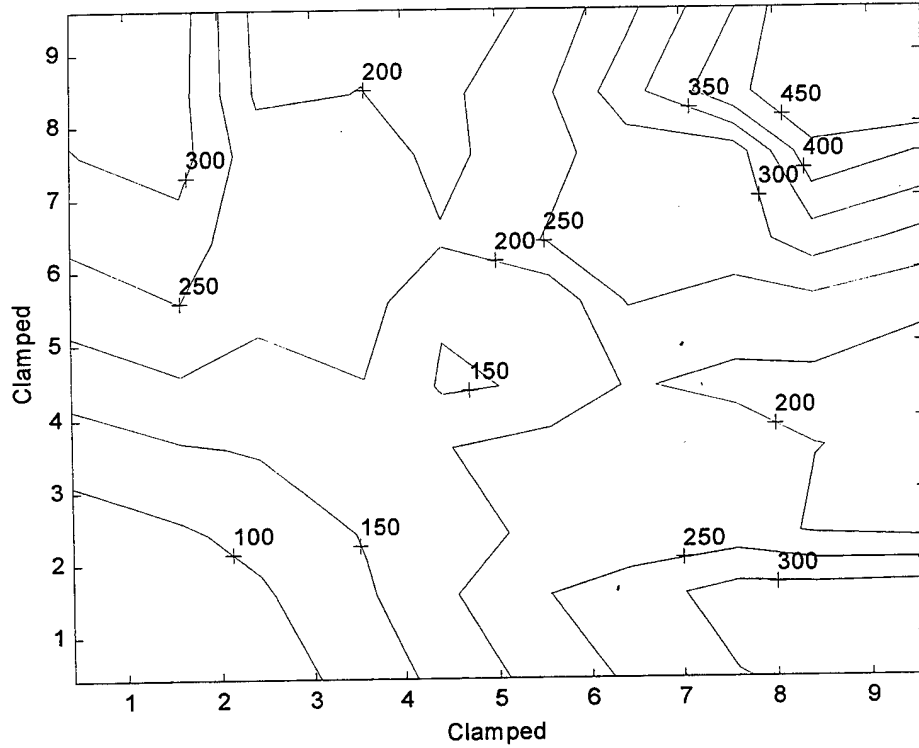


Figure 10. Square Plate, Clamped Edges, Concentrated Load at The Center, Fiber Stress Contour Plot

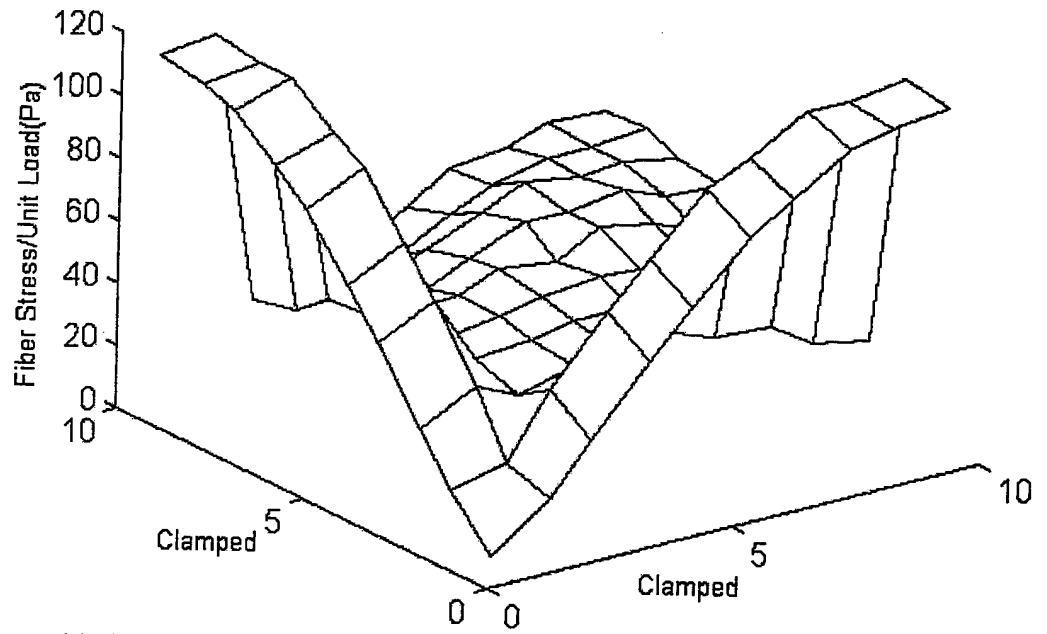


Figure 11. Square Plate, Clamped Edges, Uniformly Distributed Load, Fiber Stress Plot

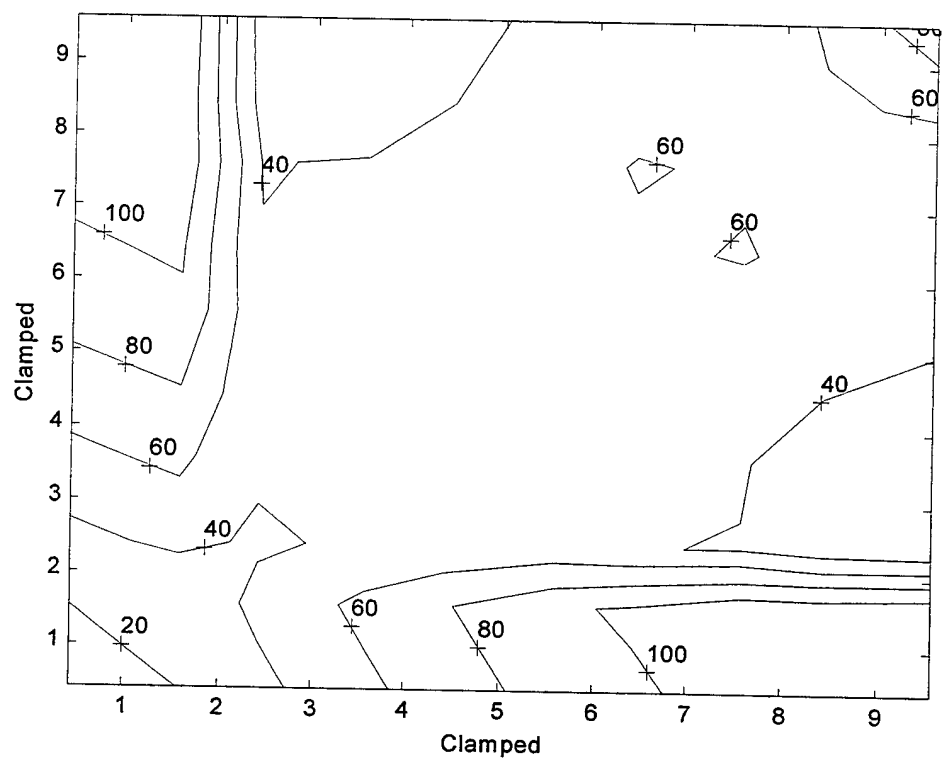


Figure 12. Square Plate, Clamped Edges, Uniformly Distributed Load, Fiber Stress Contour Plot

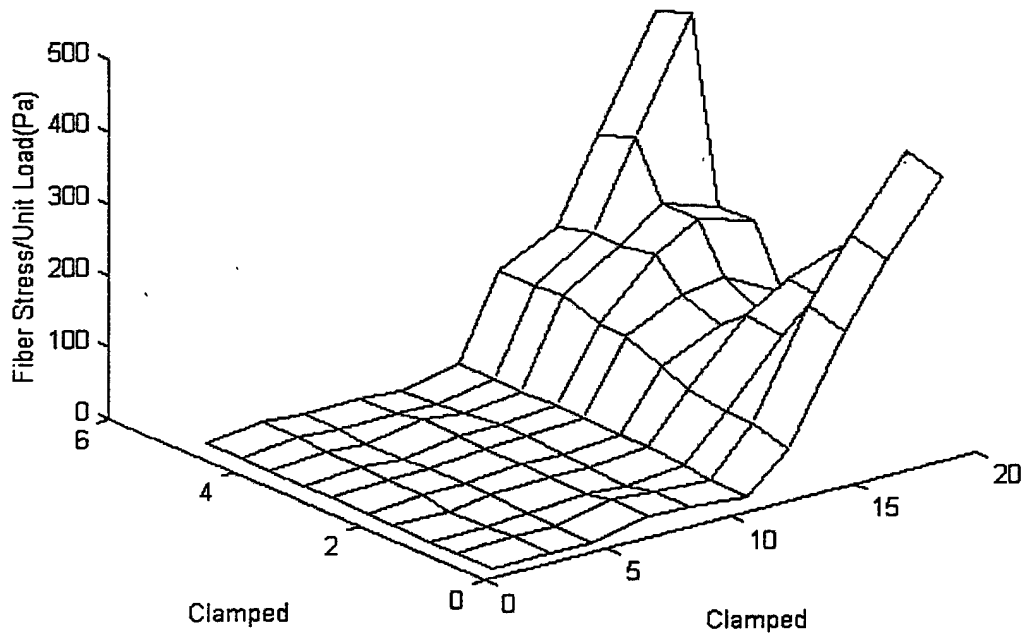


Figure 13. Rectangular Plate, Clamped Edges, Concentrated Load at The Center, Fiber Stress Plot

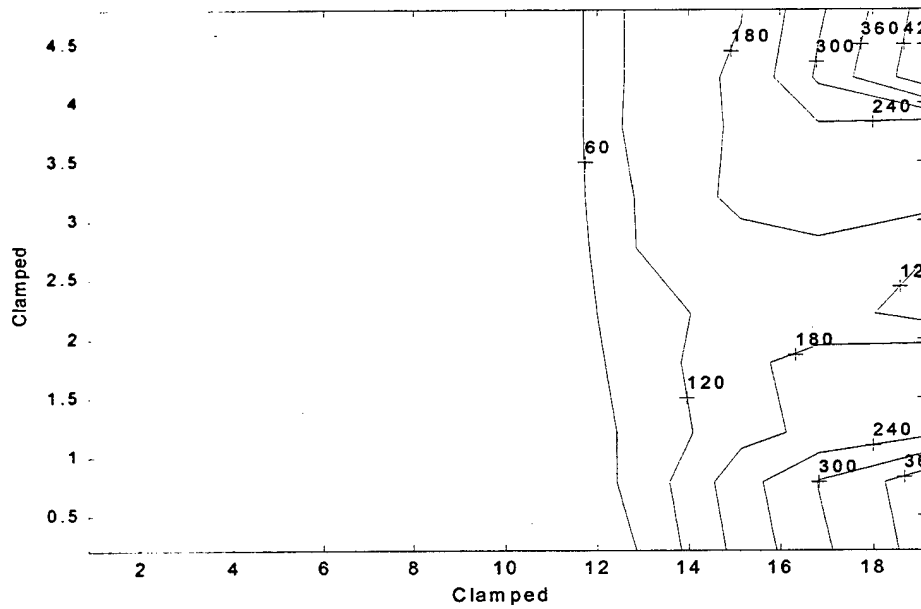


Figure 14. Rectangular Plate, Clamped Edges, Concentrated Load at The Center, Fiber Stress Contour Plot

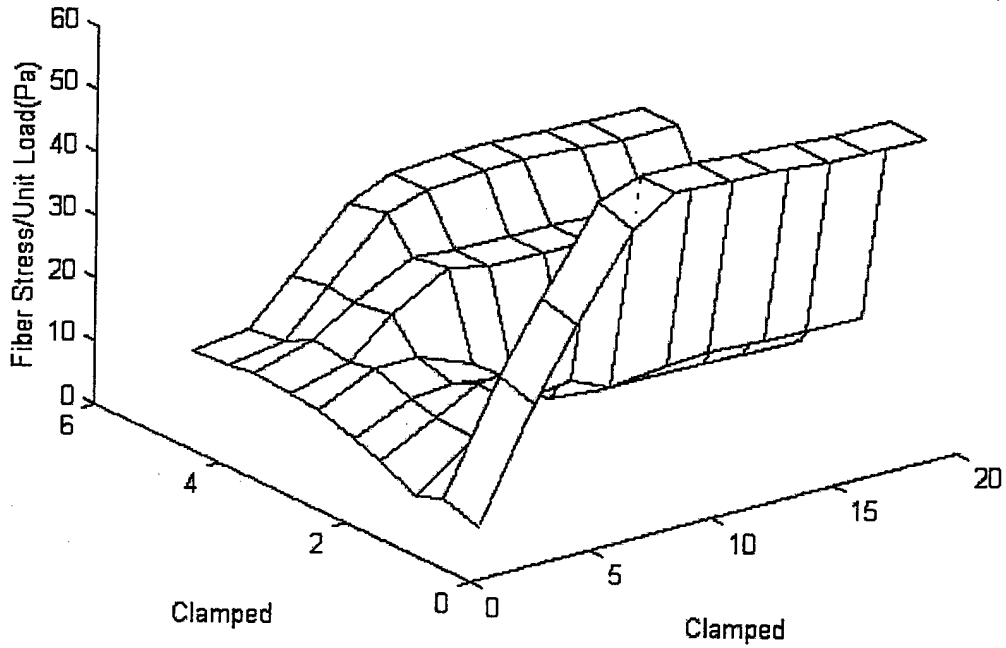


Figure 15. Rectangular Plate, Clamped Edges, Uniformly Distributed Load, Fiber Stress Plot

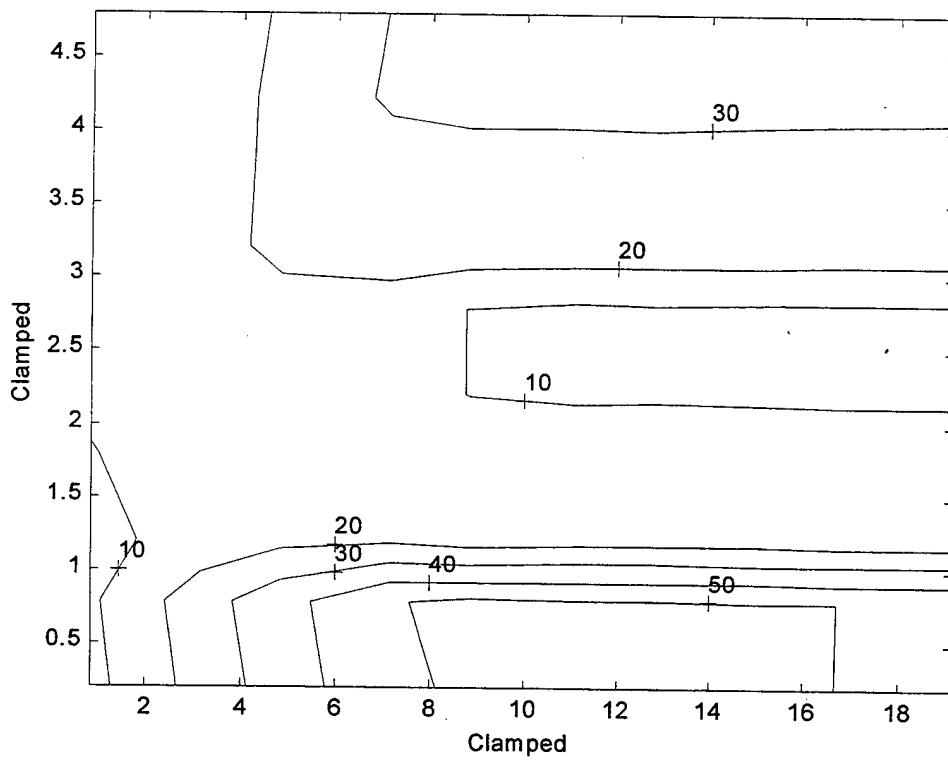


Figure 16. Rectangular, Clamped Edges, Uniformly Distributed Load, Fiber Stress Contour Plot

2. Simply Supported Plates

In the present analysis, the plates that have the same geometries, material properties, node configurations and load applications as the plates examined in the previous section are studied for simply supported edges.

For the square plate subjected to a center concentrated load with the simply supported edges, the maximum fiber stress occurs at the center of the plate where the load is applied. The minimum stress occurs at the midpoints of the symmetric edges. Due to the symmetric boundary conditions and equal length of the edges, the stress distribution shows a symmetric behavior with respect to its diagonal of the plate. The stress distribution for the concentrated center load is shown in Figures 17-18.

For the distributed load, the maximum stress occurs along a region, instead of just at one point. This region is just like a canal along the diagonal of the plate. The stress is distributed symmetrically with respect to the diagonal of the plate again. The stress distribution for the distributed load is shown in Figures 19-20.

Rectangular plates with simply supported edges show the maximum fiber stress at the center of the plates for both distributed and concentrated loads. The fiber stress decreases with distance from the center in all directions, and finally becomes zero at the corners and midpoints of the edges. The concentrated load results in faster decrease of the fiber stress from the center than the uniform pressure load.

For both rectangular and square plates, the concentrated load at the center creates stress values that are five times greater than the stress values created by distributed loads. The stress distributions are shown in Figures 21-24.

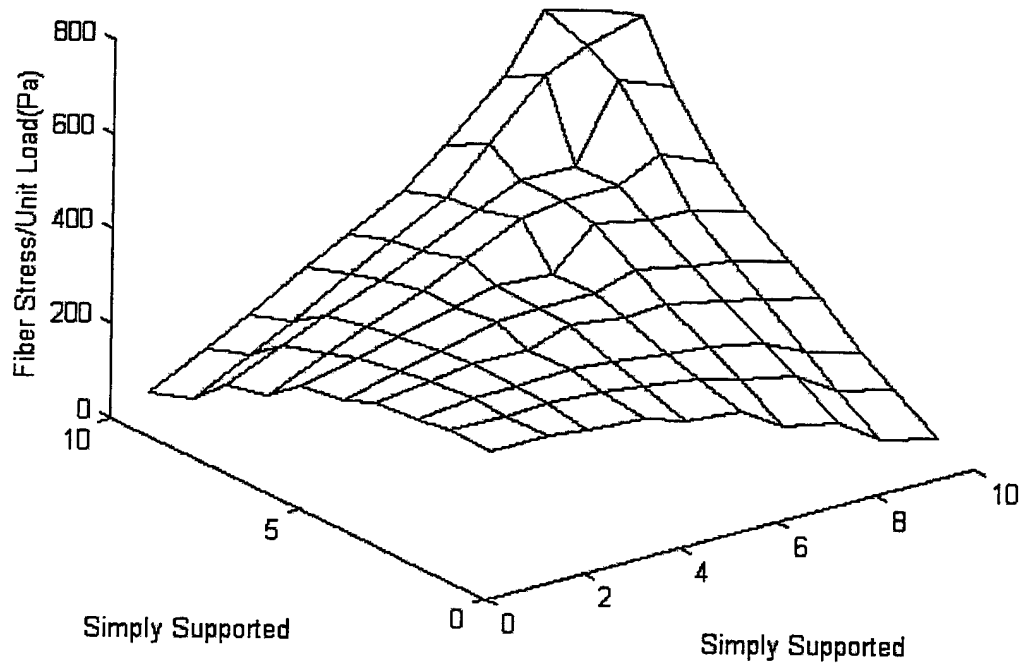


Figure 17. Square Plate, Simply Supported Edges, Concentrated Load at The Center, Fiber Stress Plot

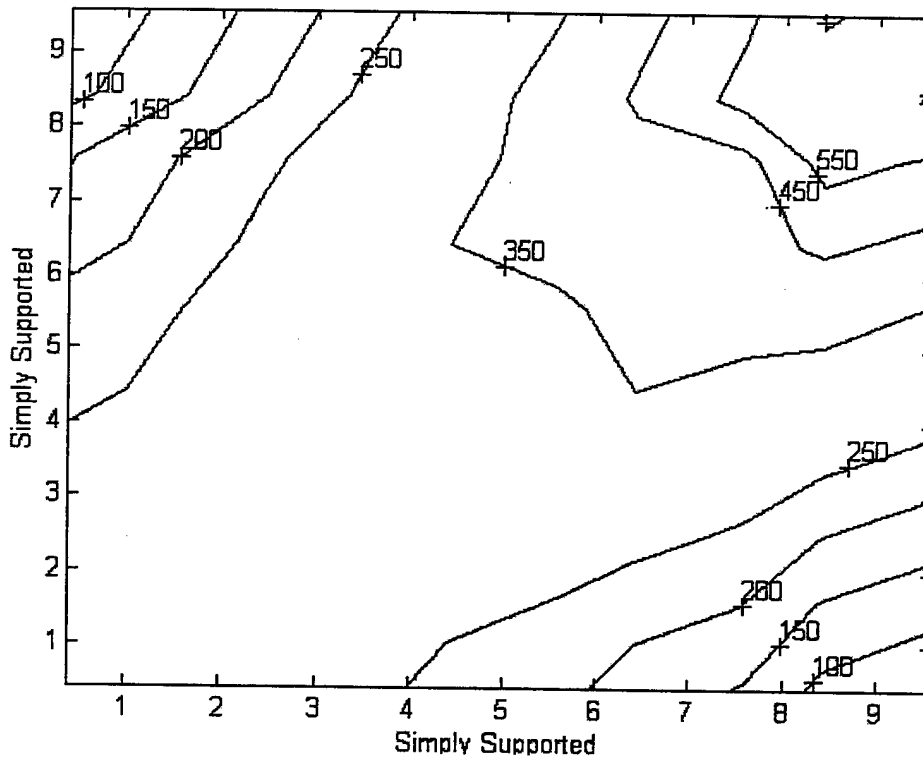


Figure 18. Square Plate, Simply Supported Edges, Concentrated Load at The Center, Fiber Stress Contour Plot

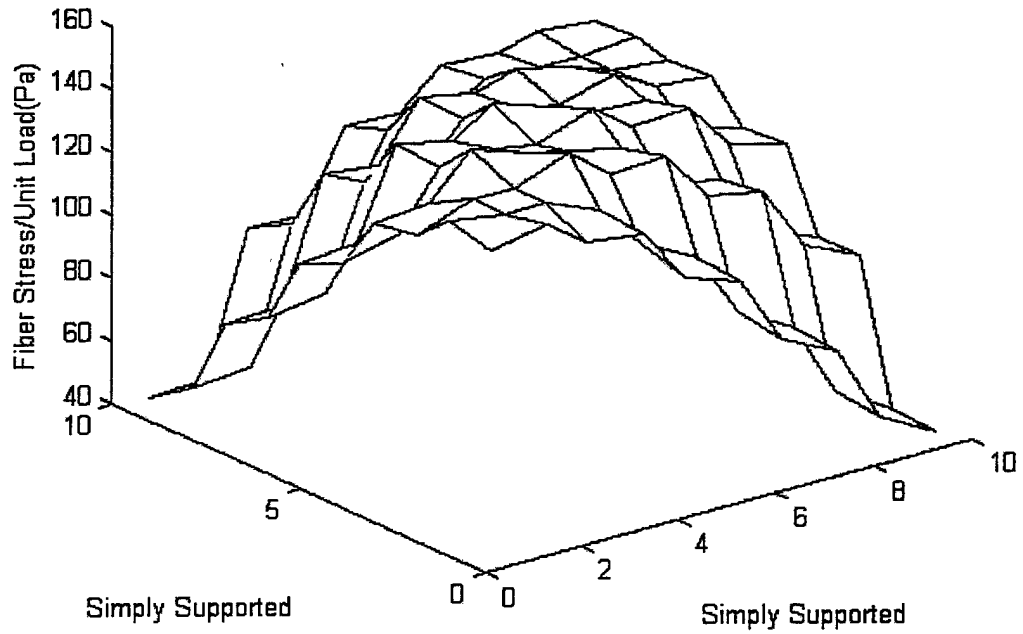


Figure 19. Square Plate, Simply Supported Edges, Uniformly Distributed Load, Fiber Stress Plot

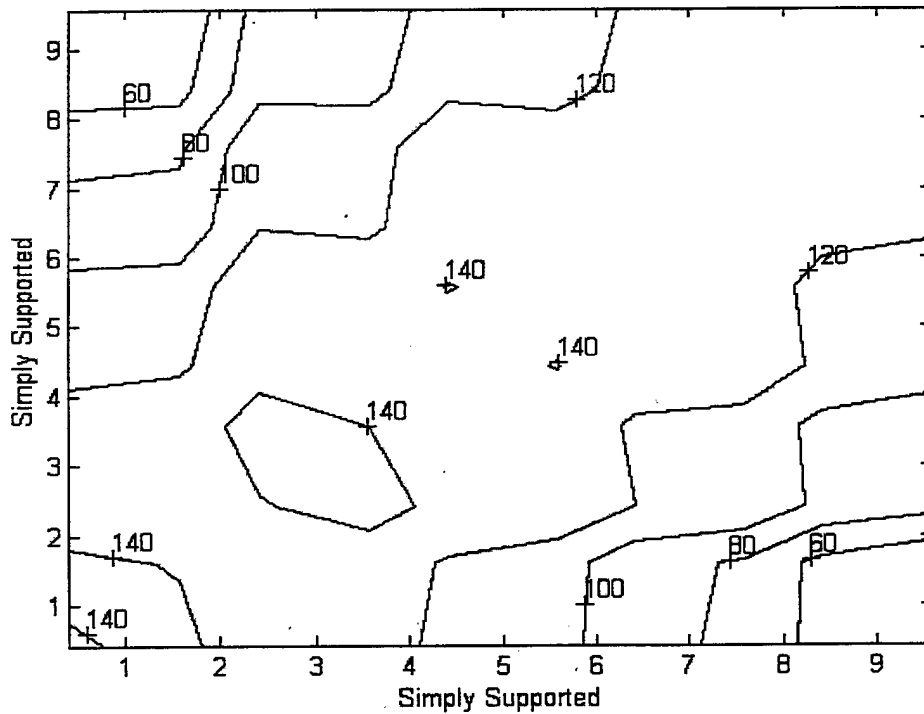


Figure 20. Square Plate, Simply Supported Edges, Uniformly Distributed Load, Fiber Stress Contour Plot

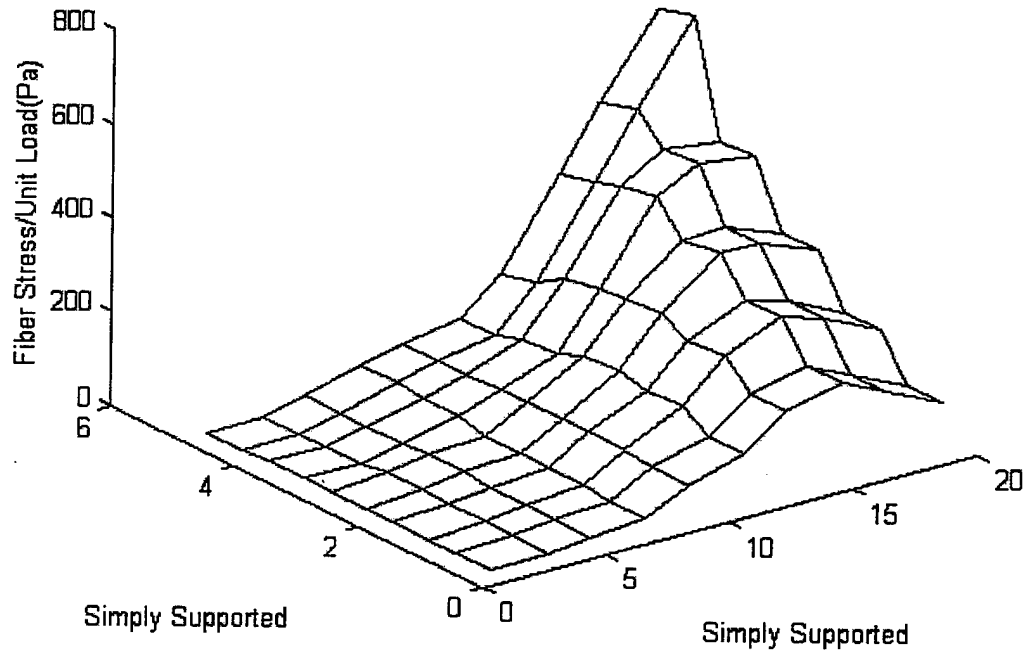


Figure 21. Rectangular Plate, Simply Supported Edges, Concentrated Load at The Center, Fiber Stress Plot

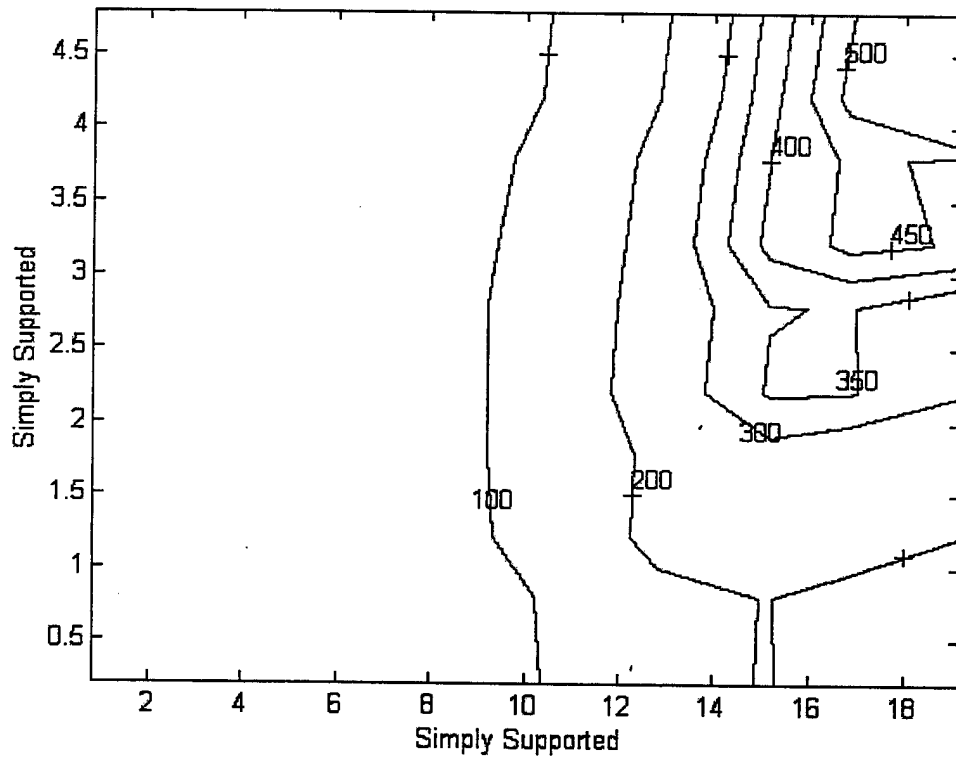


Figure 22. Rectangular Plate, Simply Supported Edges, Concentrated Load at The Center, Fiber Stress Contour Plot

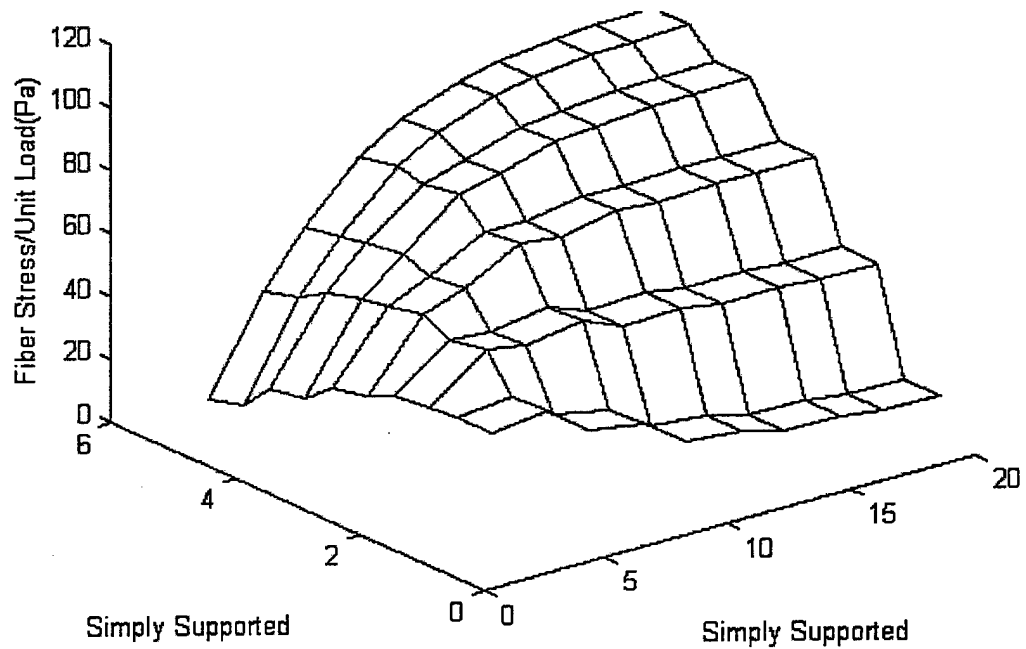


Figure 23. Rectangular Plate, Simply Supported Edges, Uniformly Distributed Load, Fiber Stress Plot

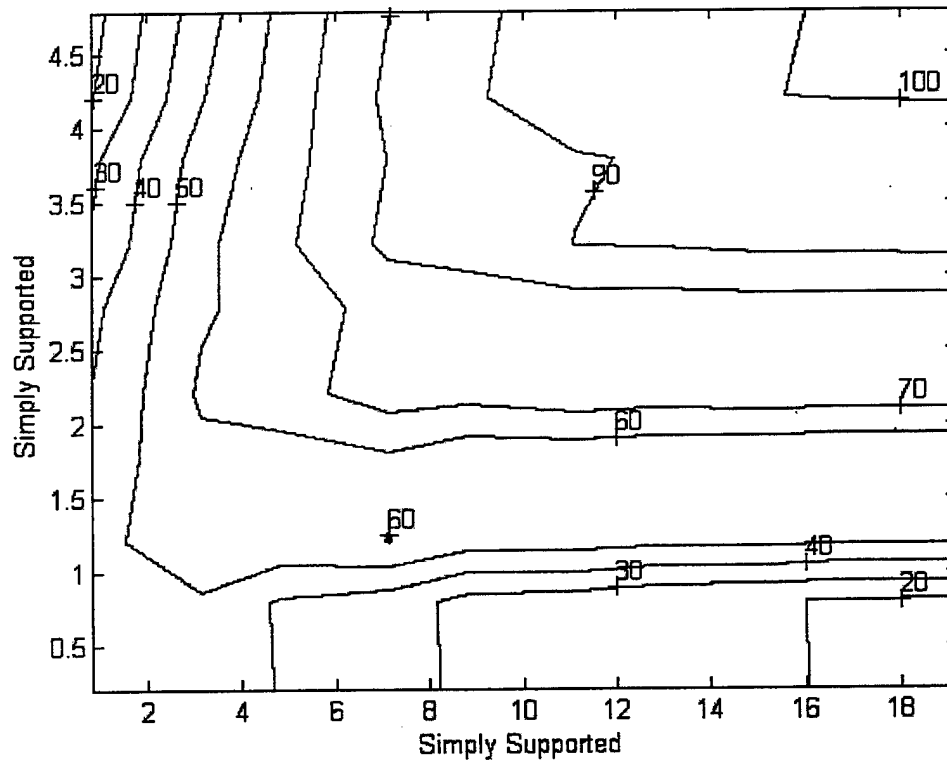


Figure 24. Rectangular Plate, Simply Supported Edges, Uniformly Distributed Load, Fiber Stress Contour Plot

C. EFFECTS OF E_f , V_s^F , AND θ_U ON THE MAXIMUM FIBER STRESS

In this section the effects of fiber elastic modulus (E_f), fiber volume fraction of the strand (V_s^F) and the undulation angle (θ_U) on the maximum fiber stress are examined. For the present analyses, square plates of woven fabric composite materials with clamped edges and the concentrated center load are tested.

As the elastic modulus of the fiber is increased gradually, maximum fiber stresses are computed. The result is plotted in Figure 25. The graph is normalized with respect to the elastic modulus of the fiber in Table 1, and the maximum stress value in Figure 9, respectively. As the fiber modulus increases by 10 times, the maximum fiber stress increases more than 40 percent.

Because the fibers are major load carrying members, higher fiber modulus makes fibers carry more stresses with decreasing stresses on the matrix material. The maximum fiber stress increases nonlinearly with the increasing fiber modulus. As the fiber modulus to the matrix modulus ratio increases, the effect of fiber modulus is smaller on the maximum fiber stress.

Figure 26 shows the fiber stress variation as a function of the fiber volume fraction of the strand. The maximum fiber stress decreases with a smooth nonlinearity with increasing fiber volume fraction.

Figure 27 shows the maximum fiber stress variation in terms of the undulation angle of the plain weave composite. Undulation angle is the angle that a yarn makes with the horizontal axis at the interlaced regions. The higher the undulation angle is, the higher the maximum fiber stress becomes. The relationship is approximately linear.

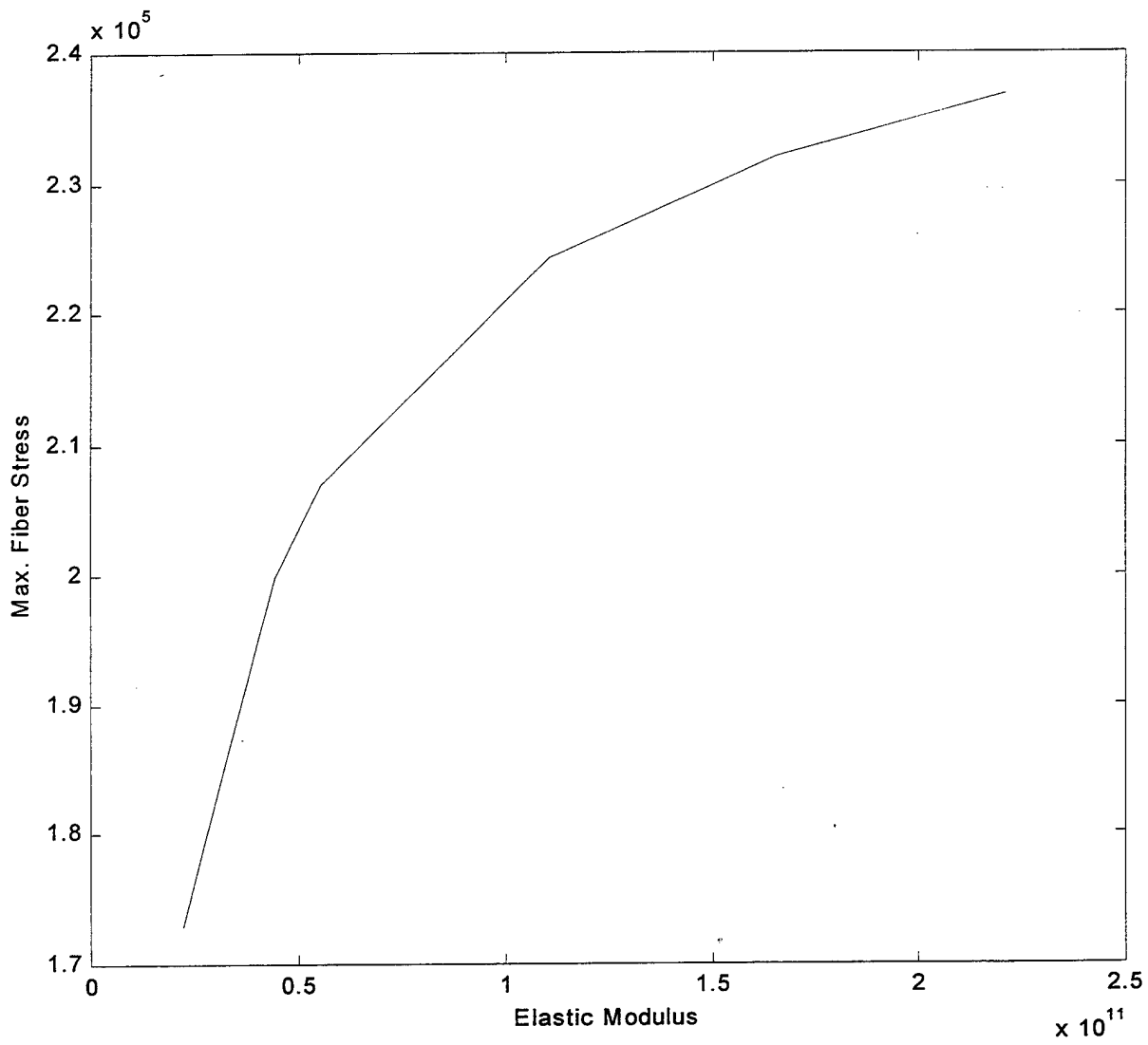


Figure 25. Elastic Modulus vs. Maximum Fiber Stress

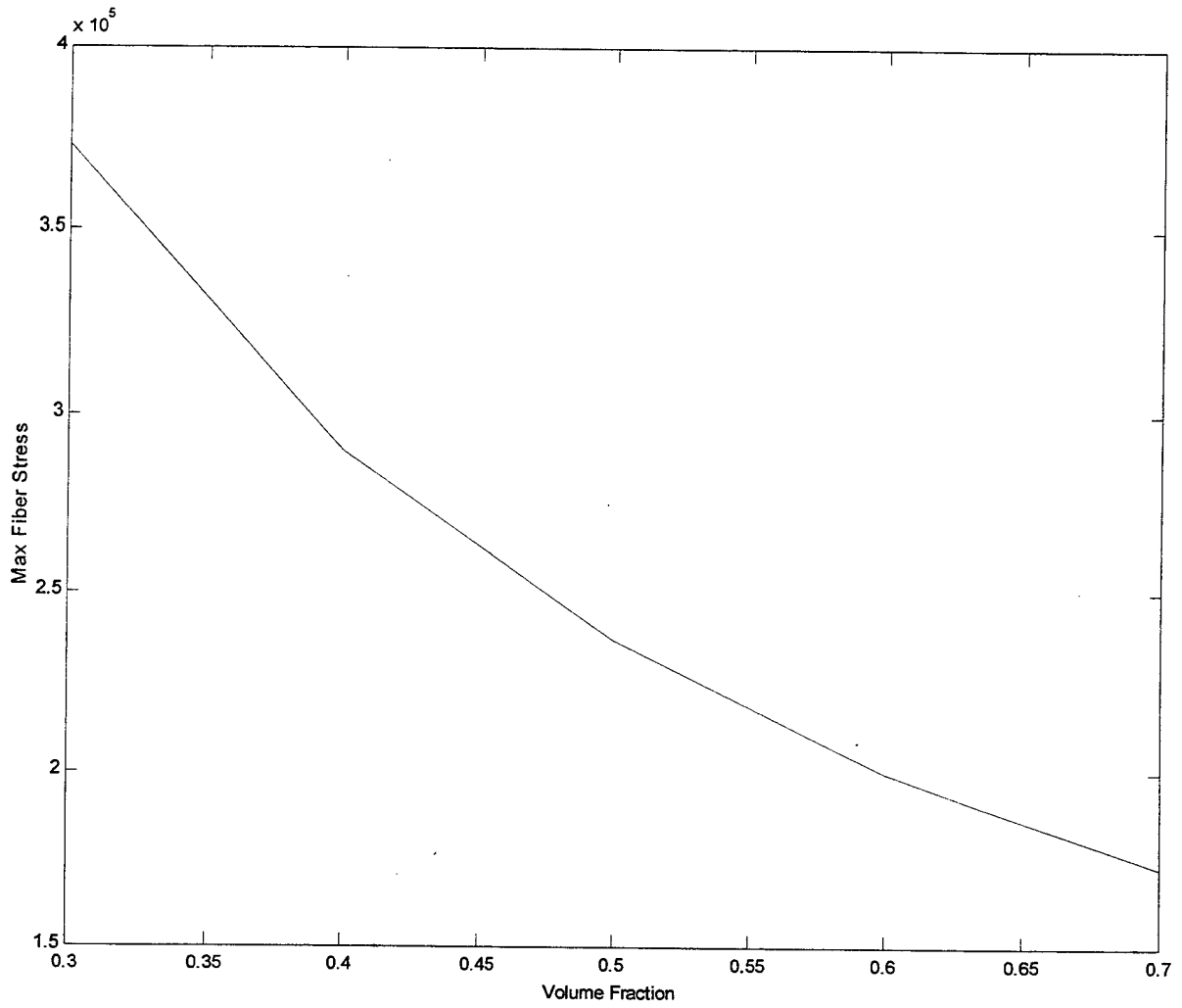


Figure 26. Fiber Volume Fraction vs. Maximum Fiber Stress

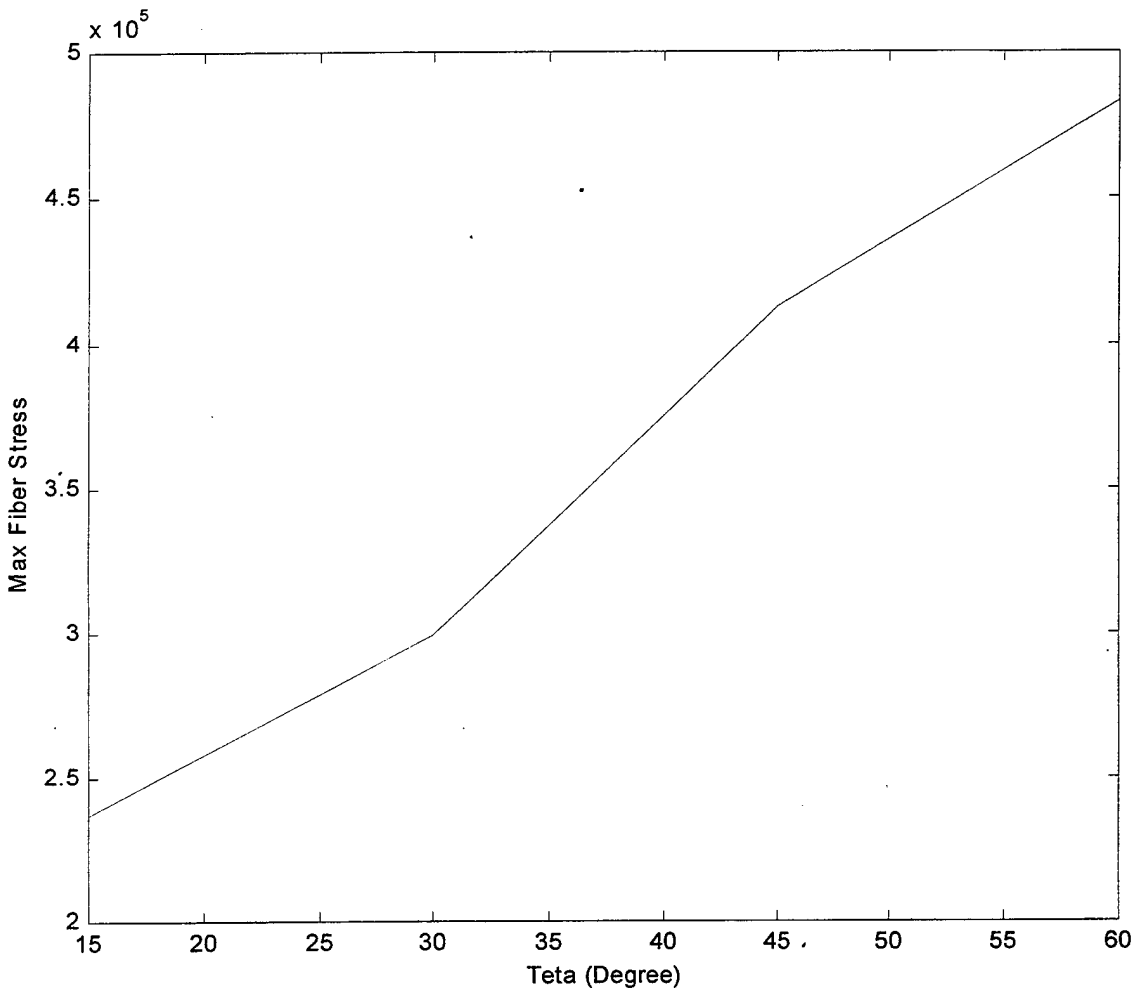


Figure 27. Undulation Angle vs. Maximum Fiber Stress

D. FAILURE PROGRESS

In this section of the study, the square plates studied in the previous sections are examined for the failure progress. Most of the plates show that when the failure initiates at the point of plate bearing the greatest fiber stress, such failure progresses catastrophically with load transfer between the failed zones and adjacent zones. Once the adjacent zones carry an extra load due to the failed zone, the neighboring zones start to fail.

For the square plate with simply supported edges and uniformly distributed load, as shown in Figures 28 and 29, the maximum fiber stress is experienced along the diagonal direction between the center and the corner. When this fiber stress value reaches the failure strength, it will cause the structure to fail along the diagonal.

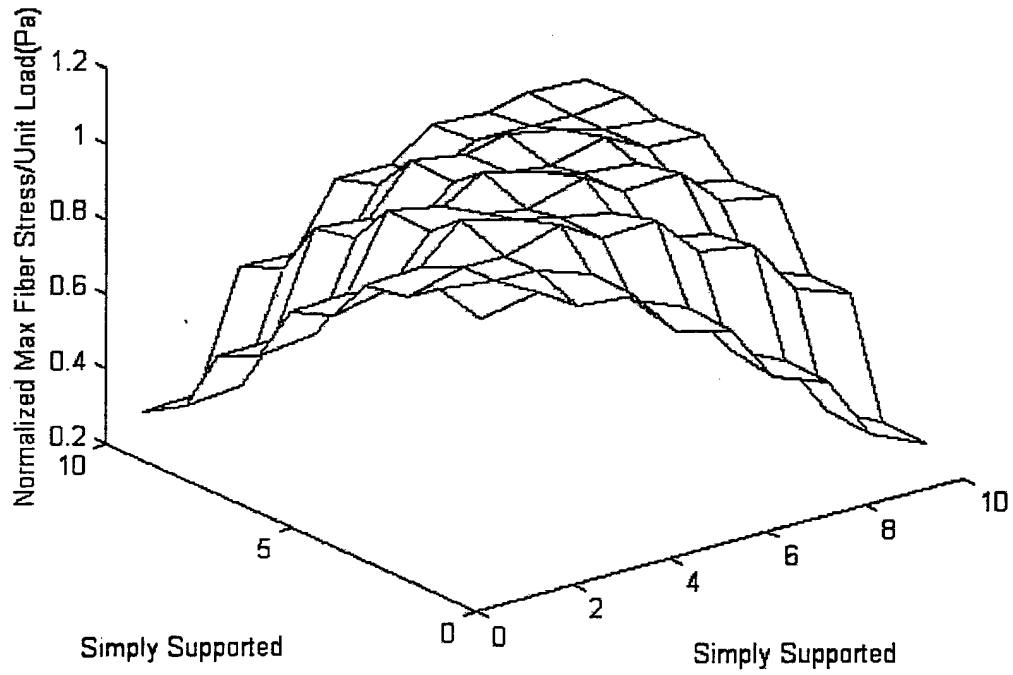


Figure 28. Maximum Fiber Stress Occurs at the Center and Failure Initiates at That Point

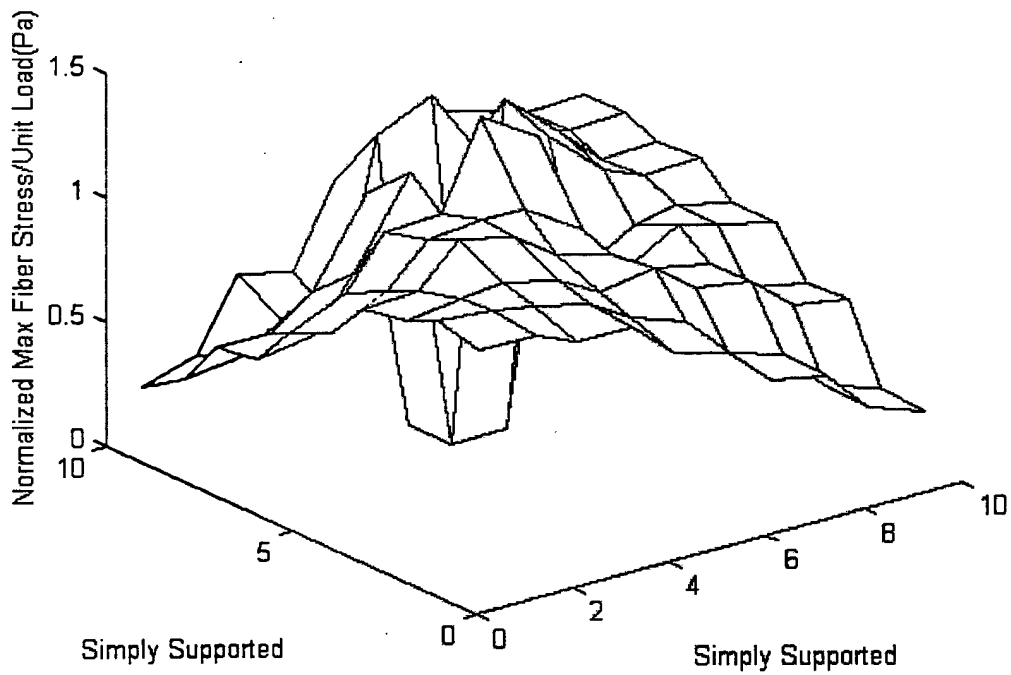


Figure 29. Failure at The Center Gets Bigger Catastrophically and The Whole Structure Fails

E. SHELL STRUCTURES SUBJECTED TO BENDING LOADS

In this section, cylinder-shaped woven fabric shell structures, subjected to concentrated loads, are examined for fiber stress distribution along the structure. Fiber and matrix materials are the same as in the previous sections, and fiber volume fraction is 0.5. For this set of studies, one edge of the cylinder is clamped and one of the corners on this edge has a notch. The notch is of square shape and its size is $1/10$ of the cylinder edge. The structure is meshed with 400 (20X20) four-noded quadrilateral elements. The concentrated load is applied at 3 different points. The mesh generation and load application points are shown in Figure 30. For three different points of load application, the fiber stress distributions along the structure can be seen in Figures 31-33.

The load applied at the corner just above the notch (point P1) creates the maximum fiber stress at the corner of the notch. The fiber stress decreases with distance until reaching the $3/5$ of the clamped edge and increases again towards the other corner of the clamped edge. The fiber stress at load application point is $1/5$ of the maximum fiber stress at the notch. The stress distribution can be seen on Figure 31.

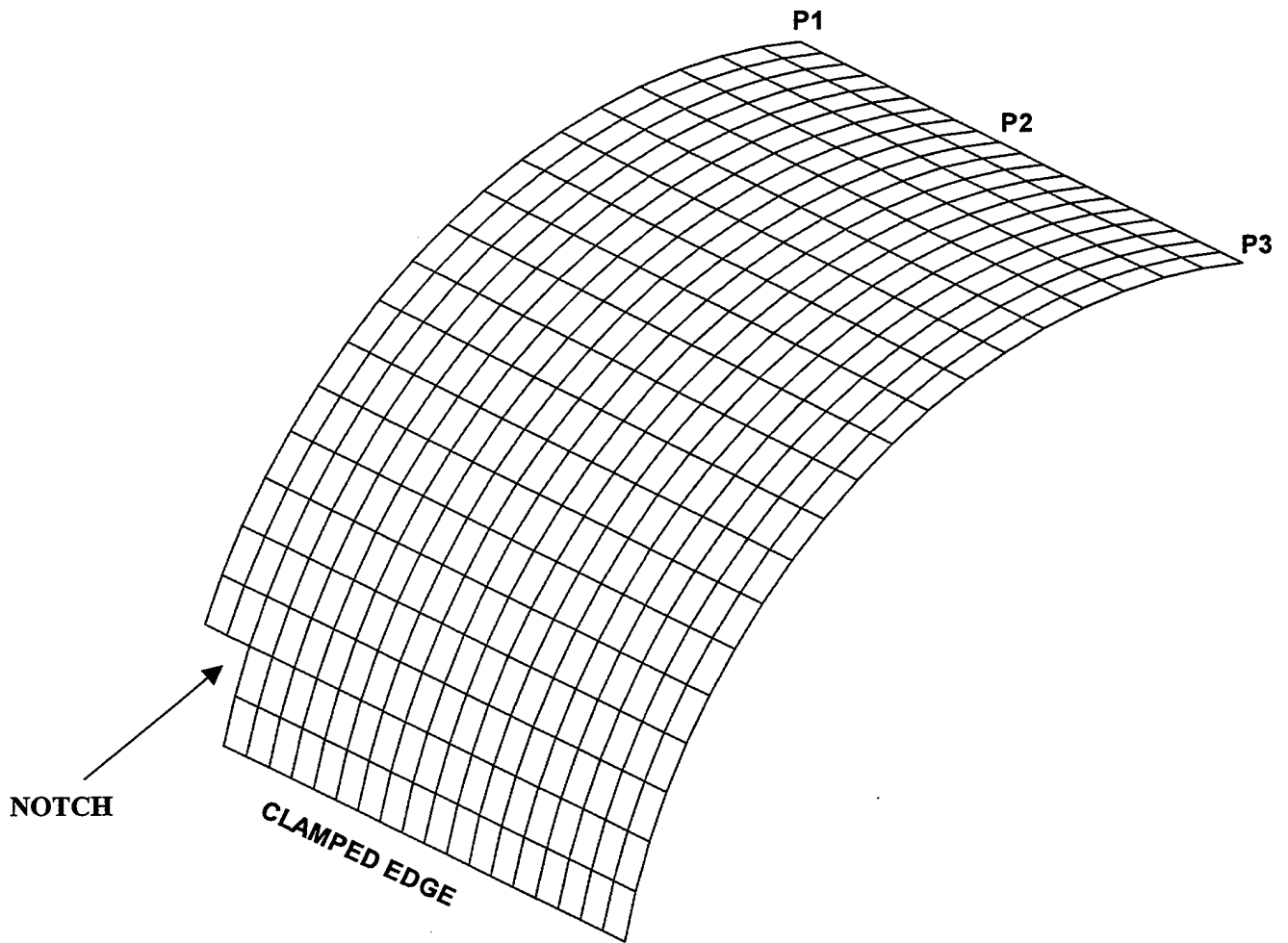


Figure 30. Cylinder Shaped Shell Structure Meshed with 400(20x20) Equilateral Elements



Figure 31. Fiber Stress Distribution Along The Cylinder-Shaped Structure, Bending Load at Point P1

The load at the center of upper edge (point P2) again creates the maximum fiber stress at the corner of the notch. The fiber stress at the load application point is $1/2$ of the maximum fiber stress. The fiber stress decreases with distance from the notch corner, and the stress is distributed symmetrically around the load application point. The stress distribution can be seen in Figure 32.

The load applied at the corner furthest from the notch (point P3) creates the maximum stress at the closest point to the load along the clamped edge. The fiber stress at the notch corner is $1/2$ of the maximum fiber stress and the fiber stress at the load application point is $1/5$ of the maximum fiber stress. The fiber stress distribution is shown on Figure 33.

The maximum stress value and location change according to the load application points. As the loads get closer to the notch corner, the maximum fiber stress increases around the notch.

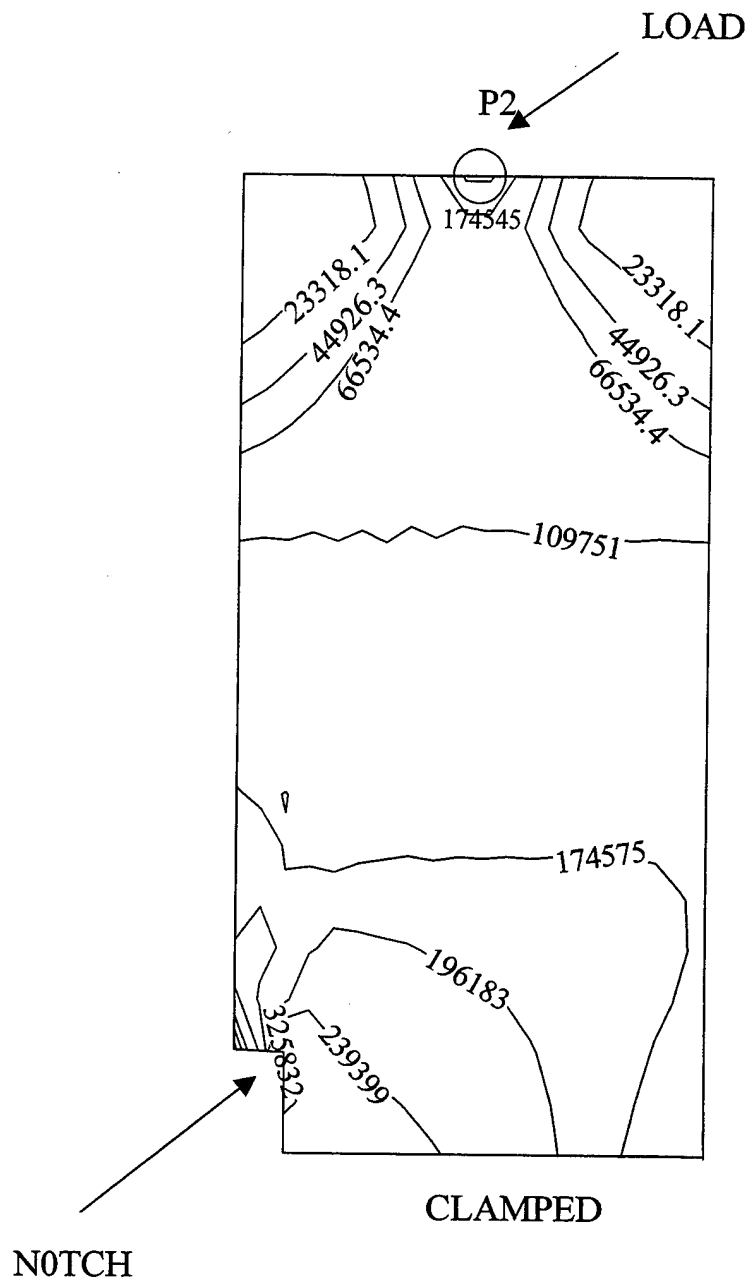


Figure 32. Fiber Stress Distribution Along The Cylinder-Shaped Structure, Bending Load at Point P2

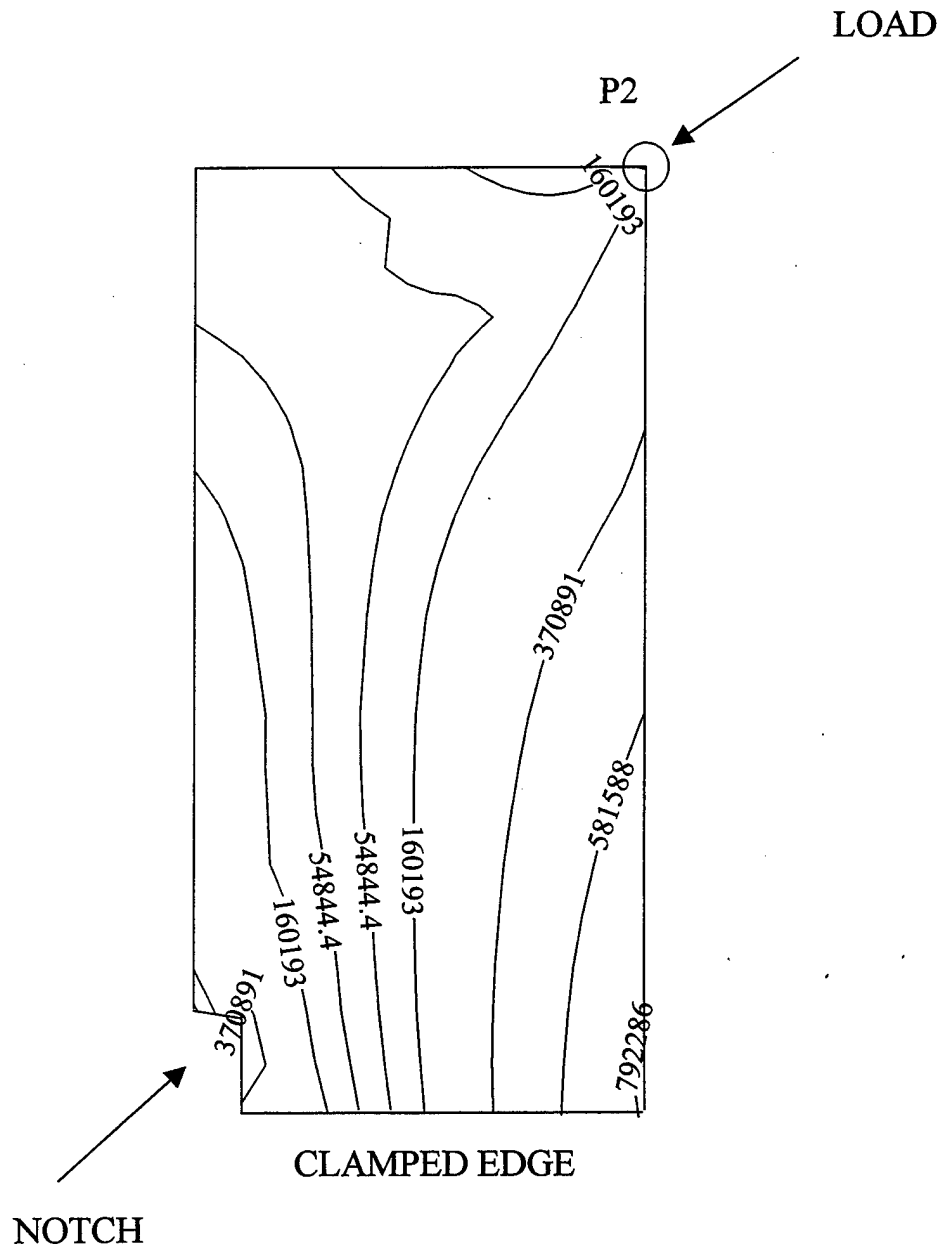


Figure 33. Fiber Stress Distribution Along The Cylinder Shaped Structure, Bending Load at Point P3

THIS PAGE INTENTIONALLY LEFT BLANK

VI. CONCLUSION AND RECOMMENDATIONS

A multi-level technique for woven composite materials is presented in this study. The technique can be used for simulation of progressive failure in woven fabric composite to predict residual stiffness and strength along with the progressive failure. The results of effective stiffness and strength computations for woven composite materials with multi-level technique are in good agreement with data obtained from experiments and other finite element analyses.

Woven fabric composite plates subjected to in-plane loads and bending loads and woven fabric shell structures subjected to bending loads are studied parametrically. The longitudinal fiber stresses are computed using the multi-level technique, because those fibers are major load carrying elements. The important results of parametric studies for the variation of fiber stresses are summarized in the following. These results demonstrate the usefulness of the proposed multi-level approach for computational modeling and simulation of woven fabric composite structures.

1. Plates with different geometrical shapes and load applications result in different maximum fiber stress values and fiber stress distributions. Concentrated loads always create greater maximum fiber stress values than the maximum fiber stress values created by distributed loads.
2. An increase in elastic modulus and undulation angle increases the maximum fiber stress. However an increase in fiber volume fraction decreases the maximum fiber stress.
3. For the plate, when failure is initiated at a certain part of the plate, bearing the greatest fiber stress, failure progress catastrophically with load transfer between the failed

zones and adjacent zones. Once the adjacent zones carry extra load due to the failed zone, the neighboring zones begin to fail again.

4. For the shell structures, which have notches, the maximum stress value and location change according to the distance between the load application point and the notch.

This study can be extended to model other types of woven fabric composites such as twill weave and four harness satin woven composites. Different plate and shell structures may be analyzed with different boundary conditions. Some experimental work is recommended to evaluate the analytical study conducted here

LIST OF REFERENCES

- [1] Ishikawa, T. and Chou, T.-W., "One-Dimensional Micromechanical Analysis of Woven Fabric Composites", *AIAA Journal*, Vol. 21, No. 12, pp. 1714-1721.
- [2] Ishikawa, T. and Chou, T.-W., "Stiffness and Strength Behavior of Woven Fabric Composites", *J. Materials Science*, Vol. 17, 1982, pp. 3211-3220.
- [3] Scida, D., Aboura, Z., Benzeggagh, M. M., and Bocherens, E., "A Micromechanics Model for 3D Elasticity and Failure of Woven-Fibre Composite Materials", *Composite Science and technology*, Vol. 59, 1999, pp. 505-517.
- [4] Hahn, H. T. and Pandey, R., "A Micromechanics Model for Thermomechanical Properties of Plain Weave Fabric Composites", *J. Engng Materials and Technology*, Vol. 116, 1994, pp. 517-523.
- [5] Aitharaju, V. R. and Averill, R. C., "Three-Dimensional Properties of Woven-Fabric Composites", *Composite Science and technology*, Vol. 59, 1999, pp. 1901-1911.
- [6] Zhang, Y. C. and Harding, J., "A Numerical Micromechanics Analysis of the Mechanical Properties of a Plain Weave Composite", *Computers & Structures*, Vol. 36, No. 5, 1990, pp. 839-844.
- [7] Naik, N. N. and Shembekar, P. S., "Elastic Behavior of Woven Fabric Composites: I-Lamina Analysis", *J. Composite Materials*, Vol. 26, No. 15, 1992, pp. 2196-2225.
- [8] Naik, N. N. and Shembekar, P. S., "Elastic Behavior of Woven Fabric Composites: II-Laminate Analysis", *J. Composite Materials*, Vol. 26, No. 15, 1992, pp. 2226-2246.
- [9] Vandeurzen, P.h., Ivens, J., and Verpoest, I., "Micro-Stress Analysis of Woven Fabric Composites by Multilevel Decomposition", *J. Composite Materials*, Vol. 32, No. 7, 1998, pp. 623-651.
- [10] Tsai, S. W. and Hahn, H. T., *Introduction to Composite Materials*, Technomic Publishing Co., Westport, Connecticut, 1980.
- [11] Gibson, R. F., *Principles of Composite Material Mechanics*, McGraw-Hill, New York, 1994.
- [12] Aboudi, J., "Micromechanical Analysis of Composites by the Method of Cells", *Appl. Mech. Rev.*, Vol. 42, 1989, pp. 193-221.

- [13] Kwon, Y. W. and Kim, C., "Micromechanical Model for Thermal Analysis of Particulate and Fibrous Composites", *J. Thermal Stresses*, Vol. 21, 1998, pp. 21-39.
- [14] Kwon, Y. W., "Calculation of Effective Moduli of Fibrous Composites with or without Micromechanical Damage", *Composite Structures*, Vol. 25, 1993, pp. 187-192.
- [15] Kwon, Y. W. and Berner, J. M., "Micromechanics Model for Damage and Failure Analyses of Laminated Fibrous Composites", *Engng Fracture Mechanics*, Vol. 52, 1995, pp. 231-242.
- [16] Pecknold, D. A. and Rahman, S., "Micromechanics-Based Structural Analysis of Thick Laminated Composites", *Computers and Structures*, Vol. 51, No. 2, 1994, pp. 163-179.
- [17] Garnich, M. R. and Hansen, A. C., "A Multicontinuum Theory for Thermal-Elastic Finite Element Analysis of Composite Materials", *J. Composite Materials*, Vol. 31, No. 1, 1996, pp. 71-86.
- [18] Garnish, M. R. and Hansen, A. C., "A Multicontinuum Approach to Structural Analysis of Linear Viscoelastic Composite Materials", *J. Applied Mechanics*, Vol. 64, 1997, pp. 795-803.
- [19] Blacketter, D. M., Walrath, D. E., and Hansen, A. C., "Modeling Damage in a Plain Weave Fabric-Reinforced Composite Material", *J. Composites Technology and Research*, Vol. 15, No. 2, Summer 1993, pp. 136-142.
- [20] Ishikawa, T., Matsushima, M., Hayashi, Y., and Chou, T.-W., "Experimental Confirmation of the Theory of Elastic Moduli of Fabric Composites", *J. Composite Materials*, Vol. 19, No. 5, 1985, pp. 443-458.
- [21] Kwon, Y. W. and Bang, H.-C., "The Finite Element Method Using Matlab", CRC Press, Boca Raton, Florida, 2000.

INITIAL DISTRIBUTION LIST

1. Defense Technical Information Center.....2
8725 John J. Kingman Road, Suite 0944
Ft. Belvoir, VA 22060-6218
2. Dudley Knox Library.....2
Naval Postgraduate School
411 Dyer Road
Monterey, CA 93943-5101
3. Professor Young W. Kwon, Code ME/Kw.....2
Department of Mechanical Engineering
Naval Postgraduate School
Monterey, CA 93943
4. Department Chairman Code ME.....1
Department of Mechanical Engineering
Naval Postgraduate School
Monterey, CA 93943
5. Engineering and Technology Curriculum Code 34.....1
700 Dyer Rd., Building 245
Monterey, CA 93943-5100
6. Ltjg. Ahmet Altekin.....1
Eski Camii Mahallesi, Narenciye Cad.
Huzur Apt. No:18/5
Kumluca/ANTALYA/TURKEY
7. Ltjg. Orhan Barbaros Okan.....1
Engineering and Technology Curriculum Code 34
700 Dyer Rd., Building 245
Monterey, CA 93943-5100